INL/EXT-13-29581
Rev. 0

Modeling of Some Physical Properties of Zirconium Alloys for Nuclear Applications in Support of UFD Campaign

Fuel Cycle Research & Development

Michael V. Glazoff

Prepared for
U.S. Department of Energy
Used Fuel Disposition Campaign

Revision 0
August 2013
FCRD-XXX-2012-XXXXXX

INL/EXT-13-29581
Rev. 0

Modeling of Some Physical Properties of Zirconium Alloys for Nuclear Applications in Support of UFD Campaign

Error! Reference source not found.**Michael V. Glazoff**

Error! Reference source not found.**August 2013**

Idaho National Laboratory
UFD Campaign
Idaho Falls, Idaho 83415

http://www.inl.gov

Prepared for the
U.S. Department of Energy
Office of Nuclear Energy
Under DOE Idaho Operations Office
Contract DE-AC07-05ID14517

UFD Campaign

Modeling of Some Physical Properties of Zirconium Alloys for Nuclear Applications in Support of UFD Campaign

INL/EXT-13-29581
Revision 0

August 2013

Approved by:

Michael V. Glazoff
Distinguished Staff Scientist
Energy Systems Integration

August 06, 2013
Date

Steven C. Marschman
Project Manager, Field Demonstration
Storage and Transportation, Used Fuel Disposition

8-6-2013
Date

ABSTRACT

Zirconium-based alloys Zircaloy-2 and Zircaloy-4 are widely used in the nuclear industry as cladding materials for light water reactor (LWR) fuels. These materials display a very good combination of properties such as low neutron absorption, creep behavior, stress-corrosion cracking resistance, reduced hydrogen uptake, corrosion and/or oxidation, especially in the case of Zircaloy-4. However, over the last couple of years, in the post-Fukushima Daiichi world, energetic efforts have been undertaken to improve fuel clad oxidation resistance during off-normal temperature excursions. Efforts have also been made to improve upon the already achieved levels of mechanical behavior and reduce hydrogen uptake. In order to facilitate the development of such novel materials, it is very important to achieve not only engineering control, but also a scientific understanding of the underlying material degradation mechanisms, both in working conditions and in storage of used nuclear fuel.

This report strives to contribute to these efforts by constructing the thermodynamic models of both alloys; constructing of the respective phase diagrams, and oxidation mechanisms. A special emphasis was placed upon the role of zirconium suboxides in hydrogen uptake reduction and the atomic mechanisms of oxidation. To that end, computational thermodynamics calculations were conducted concurrently with first-principles atomistic modeling.

CONTENTS

FIGURES

Modeling of Some Physical Properties of Zirconium Alloys for Nuclear Applications in Support of UFD Campaign

1. INTRODUCTION

Zircaloy-2 (hereafter referred to as Zr-2) was originally developed to improve corrosion resistance of the Zircaloy-1 (i.e., Zr-2.5%Sn) [1-3, 5]. This goal was achieved by adding minor amounts of Cr, Ni, and Fe. It was used, with significant success, as the cladding material to retain nuclear fuel in boiling water reactors (BWRs) and, to a lesser extent, pressurized water reactors (PWRs). To avoid using very expensive "iodide" zirconium, zirconium sponge was recommended for alloying purposes; the Zr-2 chemical composition and the maximum level of allowable impurities (specified for reactor-grade material), are presented below, in wt.% [1, 6]:

Zr-2: Zr, (1.2-1.7)% Sn, (0.07-0.2)% Fe, (0.03-0.08)% Ni, and (0.05-0.15)% Cr. The following level of impurities is allowed for Zr-2: Al - 0.0075%; B – 0.00005%; C - 0.0270%; Cd - 0.00005%; Co - 0.0020%; Cu - 0.0050%; H - 0.0025%; Hf - 0.0200%; Pb - 0.0130%; Mg - 0.0200%; Mn - 0.0050%; N - 0.0080%; Na - 0.0020%; Si - 0.0120%.

The principal goal of these alloying elements in Zr-2 was to neutralize the detrimental effect on corrosion resistance of the impurities, especially – nitrogen, aluminum, and carbon, [1, 6]. However, this alloy had a hydrogen uptake higher than the level required for work in pressurized light water reactors, [1. It is mostly for this reason that the Zr-4 alloy was developed, [1]. The principal thought was to eliminate nickel as it demonstrated the highest ability to serve as a hydrogen getter. Consequently, its alloy composition window was selected as follows: Zr-4: Zr, (1.2-1.7) % Sn, (0.18-0.24) % Fe, (0.07-0.13)% Cr. [7]. As a result, the hydrogen uptake was reduced almost by a factor of four.

One important issue that has not received attention in the literature is: what does the expression "hydrogen uptake" actually mean? Is this the amount of hydrogen that could be dissolved in the Zr-based solid solution at a given temperature, or the overall hydrogen distributed among solid solution, precipitates of second phases (typically Zr_2M, FCC, and hexagonal C14 Laves phases [8, 9]), and the hydride phase? If the former definition is correct, then the hydride solvus curve should be different for Zr-2 and Zr-4 as a function of temperature. If, on the other hand, the term "hydrogen uptake" is related to the rate of sorption of hydrogen in a given alloy, then one needs to understand the mechanism of such adsorption impediment for Zr-4.

The issue of hydrogen is closely connected to that of zirconium alloys oxidation. As it will be demonstrated below with atomistic simulations, the formation of certain oxygen bearing zirconium compounds, especially monoclinic ZrO_2 and suboxide Zr_3O [10-12], at the interface "cooling water – alloy surface" is critical to preventing hydrogen pickup. Under normal working conditions the primary source of hydrogen is radiolysis of water. Under catastrophic temperature excursions above 800°C, zirconium will be oxidized by water forming ZrO_2 and hydrogen. We will be concerned mostly with the conditions realized during spent nuclear fuel storage, so the temperature range of interest will be below 400°C.

In general, zirconium is thermodynamically unstable with respect to its oxidation process even at room temperatures [13, 14]. The necessary condition for the ZrO_2 formation is that the partial pressure of O_2 must be higher than the dissociation pressure of the ZrO_2 at a given temperature, [13]. Since this condition is satisfied even in deep vacuum, there will always be a thin layer of oxide on the surface, of the order of 2nm to 5nm. Anoth**er source of potential problems is the metastability of Zr and its alloys with respect to oxidation by fresh** and/or spent nuclear fuel, UO_2, [14].

Consequently, in this paper a research effort was made to understand the following issues: (1). Construction of self-consistent thermodynamic models of hydrides for pure Zr, Zr-2, and Zr-4; (2). Understanding the phase equilibria and thermodynamic properties in the Zr-O system and interaction of Zr-2 and Zr-4 with oxygen, paying special attention to the role of zirconium suboxides in the overall reduction of hydrogen pickup; (3). Elucidating the role of microstructure in the reduction of hydrogen uptake; and (4). Providing specific recommendations on safe dry storage of spent nuclear fuel (SNF).

The paper is organized as follows. In Section 2, the employed computational methods, i.e., first principles atomistic simulations and computational thermodynamics of materials are described. Section 3 describes the equilibrium aspects of hydride formation in pure Zr, Zr-2, and Zr-4. Section 3 is devoted to the Zr-O system, its thermodynamic properties and phase equilibria. Special emphasis was made upon the protective role of Zr_3O in reducing the hydrogen uptake in Zr and its alloys. In Section 4 conclusions and recommendations for future research are provided.

2. OXIDATION AND HYDROGEN UPTAKE IN ZIRCONIUM, ZIRCALOY-2 AND ZIRCALOY-4: COMPUTATIONAL THERMODYNAMICS AND AB INITIO CALCULATIONS (by Michael V. Glazoff)

2.1 Computational Methods

In this work, *ab initio* first-principles, density functional theory (DFT) – based calculations and computational thermodynamics of materials (CALPHAD approach – stands for CALculation of PHAse Diagrams), [22-24]) were used. Their brief descriptions are given below.

2.1.1 Ab Initio Calculations

The supercell total energy calculations were based on the generalized gradient approximation (GGA) for exchange and correlation, and plane waves [15]. We used the GGA functional of Perdew, Burke, and Ernzerhof (PBE) [16], which gives good results for chemisorption of molecules on transition-metal surfaces and similar processes. Projected Augmented Wave (PAW) scalar relativistic pseudopotentials [17, 18], and the VASP code [19] were used. The energy cutoff for the plane-wave basis was set at 500 eV, and all integrations over the Brillouin zone were done using the Monkhorst-Pack scheme with four k points in the relevant irreducible wedge. Inclusion of additional k points was found to have minimal effect on the total energy differences of interest.

We used two hcp supercells containing 54 atoms ($3 \times 3 \times 3$ hcp unit cells) and 200 atoms ($5 \times 5 \times 4$ unit cells). For each supercell, we relaxed all the atomic positions until the quantum-mechanical force on each atom became smaller than 0.02 eV/Å. Activation barriers were calculated using the nudged-elastic-band method, [20].

2.1.2 Computational Thermodynamics of Materials

The goal of computational thermodynamics is to establish a bridge between phase equilibria and thermodynamic properties of materials. To achieve that, one needs the conditions of equilibrium, as well as certain models for all solid, liquid, and gaseous phases participating in a given equilibrium. Even if such models are reliable and physically consistent, the problem of global optimization of the system free energy has to be solved. In turn, such problems require that significant computational power and efficient optimization algorithms are available to the researcher.

All of these conditions started to be realized in the beginning of the 1980s. Mats Hillert in Sweden (KTH) [22] supervised the development of the ThermoCalc and DICTRA software. Also, Hillert made very significant contributions to a number of useful thermodynamic models (theory of sub-lattices [22], energy compound formalism, the concept of para-equilibrium, etc. [22]. Other models were developed for different types of systems, including model of ionic liquids used in this work. Lukas et al. [23], Saunders and Miedownik [24] developed the generalized equilibrium conditions, (software BINGGS for binary systems). Liu used first-principles approach to obtain data necessary for thermodynamic simulations, [25]. Similar work developed, concurrently and independently, in Canada (A.D. Pelton and software FactSage) and in the US (the late Prof. Austin Chen, software PANDAT). As a result, it became possible to provide self-consistent descriptions of phase equilibria in multi-component systems and thermodynamic properties of materials [22].

In this work, commercial databases for zirconium alloys TTZR1 (ThermoTech Ltd.) and binary alloys TCBIN (ThermoCalc AB) were used. These databases and the ThermoCalc ver. S software were used to generate data on the thermodynamic properties of hydrides, in particular, partial molar enthalpy and entropy of hydrogen. The obtained results were consistent with the constructed phase diagrams and property diagrams. All results were critically evaluated in light of the existing experimental data.

2.2 Results and Discussion

2.2.1 Zirconium Hydrides and Hydriding of Pure Zr, Zr-2, and Zr-4

The formation of hydrides and the problem of hydriding were studied very extensively, [1-3, 26]. First principles calculations of the equilibrium crystalline lattice parameters, free energy of formation at different temperatures, and the phonon density of states were discussed by Blomquist and by Zhu et al., [35, 36]. A detailed overview of the problem of hydrogen solubility in Zr and its alloys was provided by Anghel [13]. The principal reason of this interest is that the formation of zirconium hydrides may cause such undesirable phenomena as hydrogen embrittlement and reorientation of hydrides during storage that may be detrimental to the overall mechanical properties of the fuel during transportation and handling prior to disposal [37-45]. Consequently, efforts were made to reduce hydrogen uptake via changes in alloy chemical composition, development of different coatings, thermo-mechanical treatments optimizing alloy microstructure (size distribution and number density of second phase particles, or SPPs) etc. [13], This becomes even more important as fuel burnup is extended. As burnup increases, so does the amount of radiation damage to the clad and more hydrogen is taken up by the clad [46]. This can affect the mechanical properties of the clad.

Zhang and Norton [47] have concluded that the maximal hydrogen uptake sites are located on grain boundaries and/or interfaces that facilitate heterogeneous nucleation of hydride compounds. Hydrogen tends to segregate to surfaces and interfaces (grain boundaries, cracks and other defects) in Zr. These hydrogen-rich areas are possible nucleation sites for hydrides. Moreover, oxygen in the α−Zr matrix facilitates hydrogen segregation to the surfaces, [47]. Understanding the role of the different zirconium oxides and suboxides in the reduction of hydrogen uptake was the most important goal formulated in this study.

The equilibrium crystalline structures of hcp-Zr and its three hydrides are depicted in Figures 1 and 2, respectively. In all cases, the equilibrium lattice parameter(s) were determined by total energy relaxation technique of the lattice parameters and corresponding atomic positions.

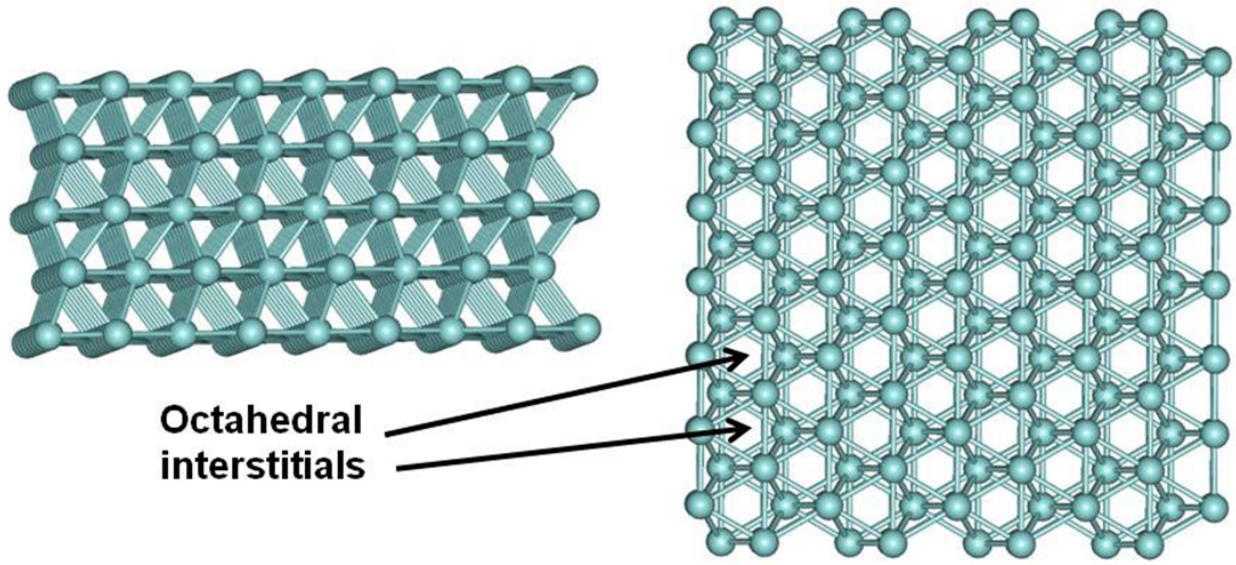

Figure 1. Hexagonal (hcp) Zr structure (different views): (a) in the direction perpendicular to the (0001) axes; (b) in the direction of the (0001) axes. Zr atoms are shown in cyan color; octahedral interstitials are indicated by arrows.

The low-temperature α−phase of Zr has hcp structure characterized by the 2/1 ratio of tetrahedral and octahedral interstitial positions per unit cell. The lattice parameters were determined in this work as a = 3.2276 Å and c = 5.1516 Å, space group P63/mmc, see Figure 1.

The transport properties (diffusion) of hydrogen and oxygen atoms in Zr are directly related to the relatively large interstitial space that could be occupied by these atoms that are nearly "free" energetically in those spaces. Figure 2 shows the relaxed atomic structures for the equilibrium positions of O and H atoms in the Zr hcp structure. Oxygen always goes into octahedral interstitials because any other possible location will inevitably damage the Zr crystalline network and cause local rearrangement of Zr atoms. Neutral hydrogen atoms may also go into octahedral interstitials (interaction energy of H atom with Zr network is below 0.1 eV, i.e., almost negligible). However, it can also position itself in the middle of Zr-Zr bonds. In the latter case, hydrogen damages the Zr network by forming asymmetric Zr-H-Zr bridges or even attaching itself to only one Zr atom and leaving dangling bond defect at another Zr atom. However, this "damage" is not that significant as it would be if oxygen atom were placed in a similar position – the energy of Zr-H-Zr configuration is only 0.5 eV higher than that of the interstitial configuration. It means that although H would energetically prefer to be located at an interstitial position, metastable Zr-H-Zr configurations are also possible if the process is driven kinetically.

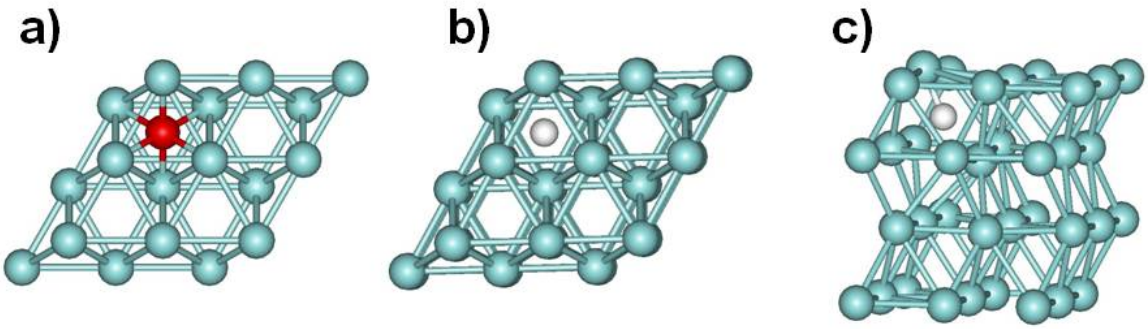

Figure 2. Positions of single oxygen and hydrogen in hexagonal (hcp) Zr structure: (a) O in the octahedral interstitial; (b) H in the octahedral interstitial; (c) H in the middle of the Zr-Zr bond. Zr atoms are shown in cyan, oxygen – in red, hydrogen – in white.

There are three distinctly different types of zirconium hydride structures described in the literature: γ–ZrH; δ–$ZrH_{1.66}$ (which was modeled in this work as $ZrH_{1.5}$) and ε–ZrH_2 [35]. In Figure 3 we present the results of our first-principles calculations yielding the three energy-relaxed crystal lattice structures.

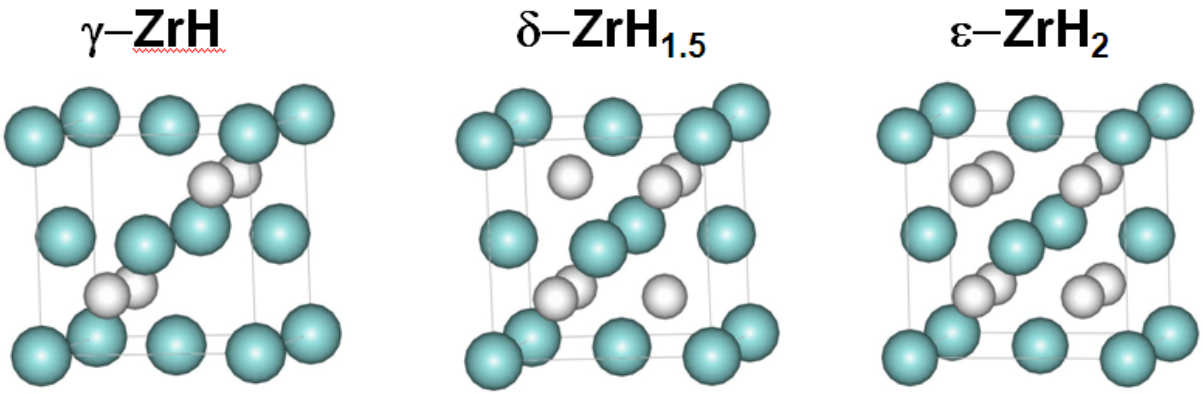

Figure 3. Relaxed crystalline structures of the three experimentally observed hydrides of zirconium: orthorhombic γ–ZrH (a=4.592 Å; c=4.492 Å); cubic δ–$ZrH_{1.5}$ (a=4.775 Å) and tetragonal ε–ZrH_2 (a=4.999 Å; c=4.433 Å).

The space groups of these hydrides are Cccm; Fm3m; and I4/mmm, respectively. It can be seen that very minor lattice distortions caused by the hydrogen atoms result in the change of the symmetry group(s) and in the value(s) of the lattice parameter(s) as one moves from one hydride to another. These results were obtained using a standard energy minimization procedure and agree well with the existing experimental data.

In Figure 4 the results of our thermodynamic modeling of the Zr-H phase diagram are presented and compared to the existing literature data, [48].

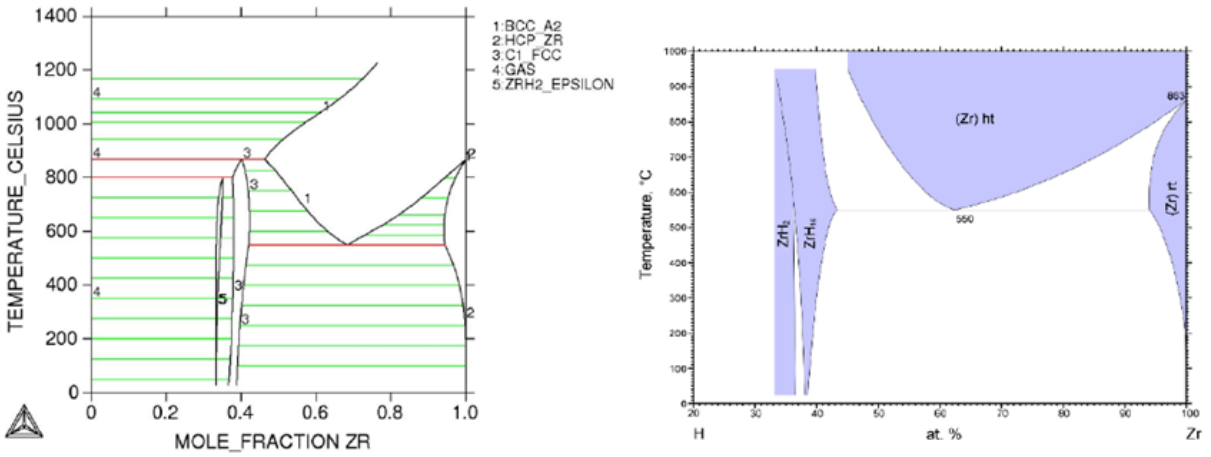

Figure 4 (a). Calculation using ThermoCalc; (b) experimental phase diagram [48]. Both diagrams agree well in establishing the phase fields of the δ- and ε-hydrides with homogeneity ranges on the basis of the stoichiometric compounds $ZrH_{1.5}$ (experimentally established value is $ZrH_{1.66}$, [35]).

The values of the Gibbs free energy computed at T=800 K are illustrated by Figure 5; these values lie in the range from -20,000 J/mol to ~ 8,000 J/mol. This reference range will be useful when we discuss existing data on partial molar enthalphy of hydrogen in different zirconium alloys, as well as for determining the driving forces of hydride formation, - the corresponding look-up tables could be used for phase-field calculations of zirconium hydride microstructure evolution.

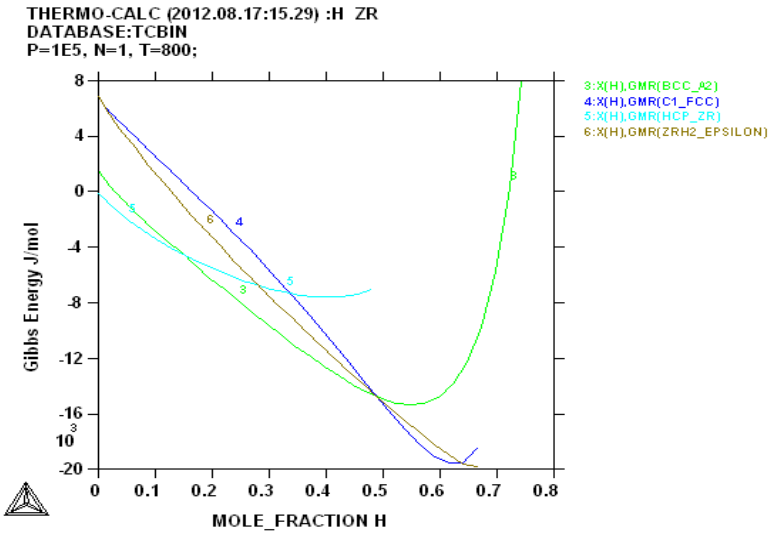

Figure 5. The Gibbs free energy of the several co-existing phases in the Zr-H systemas a function of the hydrogen mole fraction at 800 K.

The magnified diagram for the hydrogen mole fraction varying from 0 to 0.1 is given in Figure 6. It provides an estimate of the hydride dissolution temperature as 550°C corresponding to ~0.054 mole fraction of hydrogen. Also, a distinctive feature of this diagram is the retrograde solubility above 550°C, with a minimum corresponding to ~600°C. Again, these results correspond well to the existing experimental data [28, 30, and 48].

Proceeding in a similar way, we constructed the quasi-binary Zr-2 – hydrogen and Zr-4 –hydrogen property diagrams. Sometimes such diagrams are called isopleths as they correspond to

the case of constant sum of concentrations: ($n_{Zr} + n_H = const$), thus allowing variation of the hydrogen concentration at the expense of zirconium, the principal alloying element.

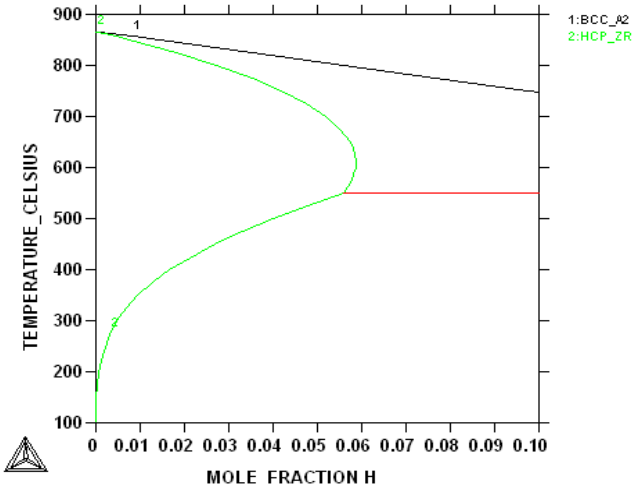

Figure 6. Fragment of the diagram in Figure 4(a) for low values of nH.

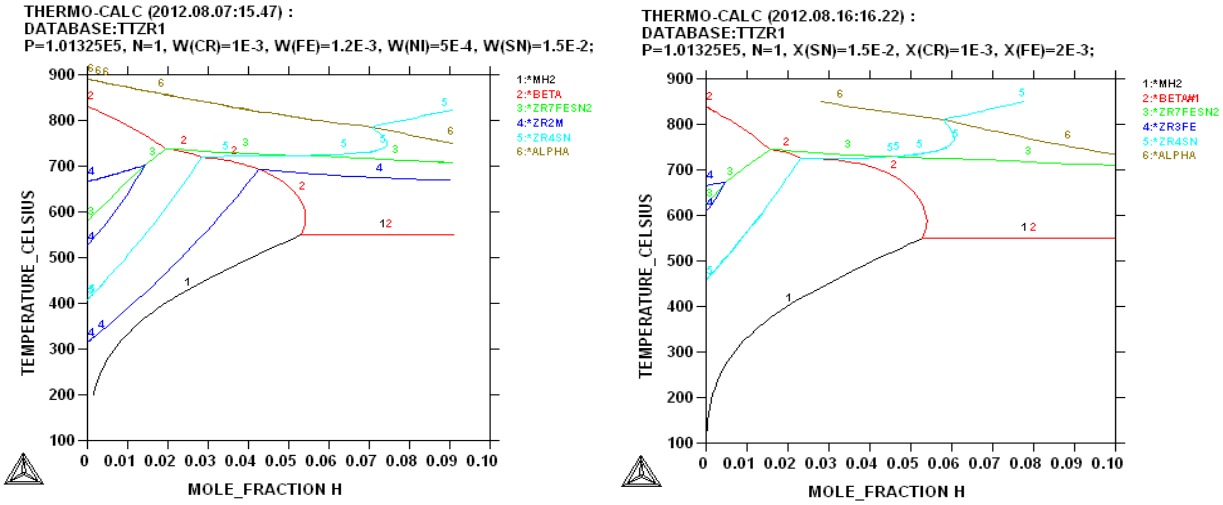

Figure 7. (a) Hydrogen isopleth for Zircaloy-2; (b) Hydrogen isopleth for Zircaloy-4

It is important to mention that in both equilibrium diagrams there are such phases present as Zr_4Sn; Zr_7FeSn_2, and Zr_3Fe, in addition to Zr_2M and hydride phase. However, Zr_4Sn and Zr_3Fe have not been discovered in the equilirium microstructure of both alloys.

Experimentally, microstructural characterization of alloy Zr-4 was conducted by Vandersande and Bement [49]. These researchers identified the second phase particles in an annealed Zr-4 sample to be primarily the hexagonal, Laves-phase C14 Zr(Fe, Cr), type. Krasevec [50] found both hexagonal and fcc Zr- and Cr-bearing precipitates, in an annealed Zr-2 sample. Mukhopadhyay et al. [51] observed fine precipitates of the two types: cubic $Zr_2(Cr,Fe)$ with a hexagonal C14 type structure (structural type $MgZn_2$) and the cubic C15-structure (prototype $MgCu_2$).

Rao and Bangaru [52] studied the microstructures of heat treated samples of Zr-4 to understand the microstructural basis of nodular corrosion. These workers used samples annealed from the beta-phase field, as-received, and samples with microstructure on the basis fo the alpha-Zr. It was established that the first group of the samples possessed the best corrosion response. An advanced synchrotron study of second-phase particles (SPPs) in bulk zirconium alloys was conducted recently by Erwin et al., [53].

The list of equilibrium phases that can be taken into consideration in the TTZR1 database, includes both the hexagonal C14 Laves phase and the C15 cubic phases, but these phases were not observed in our equilibrium calculations.

The presence of the several compounds not found in experimental phase diagrams poses a question: should we determine the hydrogen solubility from these diagrams, or from metastable diagrams in which such phases as Zr_3Fe; Zr_7FeSn_2; Zr_4Sn get the status of "suspended?" We studied both possibilities. In fact, as far as the hydride solvus and the temperature of hydride dissolution reaction are concerned, we get results almost identically similar to those for the pure Zr-H phase diagram. The temperature of the hydride dissolution reaction was 551°C for Zr-2 and 552°C – for Zr-4. Given the experimental error in determining the temperature of phase transformation is of the same order, we can conclude that these results are identical.

On the other hand, if we construct metastable phase diagrams as described above, then the highest solubility point (for hydrogen in Zr) shifts toward lower values, i.e., for both alloys ~0.034 hydrogen mole fraction. The temperature of the non-variant reaction remains the same, i.e., ~550°C.

This latter assumption contradicts the experimental evidence presented in [28] and in [30] that the equilibrium solubility maximum for Zr, Zr-2, and Zr-4 remains practically the same. In our calculations, it was around 0.058 hydrogen mole fraction for pure Zr; 0.056 – for Zr-4; and 0.054 – for Zr-2.

The thermodynamic properties evaluation for the Zr-H system was limited to the partial molar enthalpy of hydrogen in the alpha- and beta-phases. This property is very sensitive to the formation of different complexes and tendency to atomic ordering or segregation. Besides, it was evaluated experimentally and reported in at least two articles [30, 54, and 55].

The partial molar enthalpy of hydrogen in the binary Zr-H system was assessed according to the well-known expression [22]:

$$H_H = H_m + \left(\partial H_m / \partial x(Zr)\right)_{T,P} - x(Zr)\cdot\left(\partial H_m / \partial x(Zr)\right)_{T,P} \quad (1\text{-}1)$$

In expression (1), H_m stands for the molar enthalpy of the system; x(Zr) represent the molar fraction of zirconium, and H_H is the partial molar enthalpy of hydrogen for different phase fields of the diagram at 650°C.

The values of partial molar entropy of hydrogen were calculated using the following expression:

$$S_H = -\frac{\partial \mu(H)}{\partial T} \quad (1\text{-}2)$$

In expression (2) the chemical potential of hydrogen, μ(H), is assessed with respect to its references state [22].

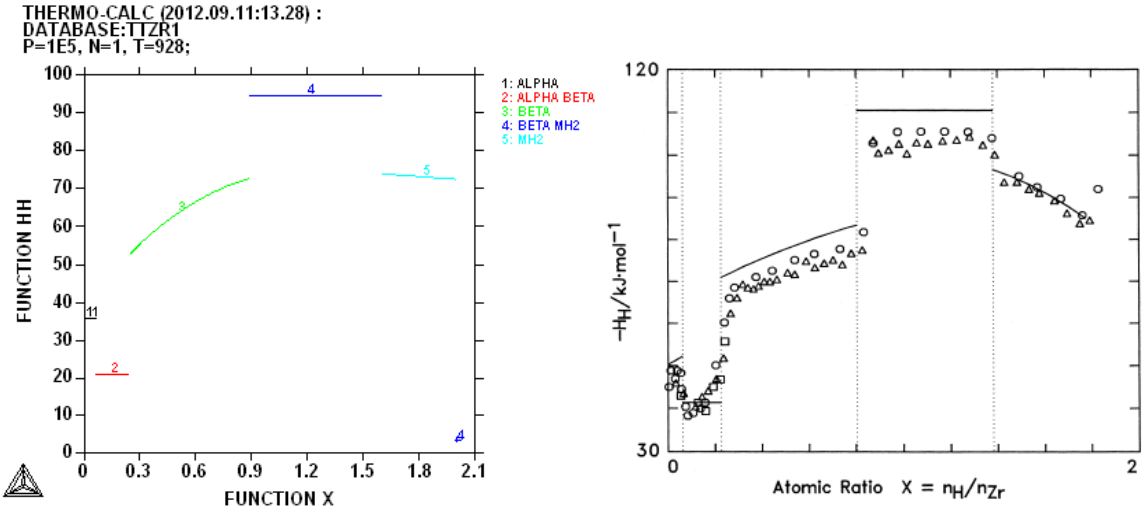

Figure 8. Partial molar enthalpy of hydrogen in different phases as a function of the x(H)/x(Zr) and its comparison to experiment [54] and the results of thermodynamic computations in [55].

The agreement between our results and the results reported in [54, 55] is quite good. At the same time, the experimental results reported in [23] give values of H_H one order of magnitude lower. For example, it was reported that for pure Zr, at temperature 650°C, H_H is around -260 kJ/mol. These results are difficult to reconcile with the ones reported in [54] and in this study. For alloys Zr-2 and Zr-4 somewhat lower values were obtained in [23]: -250 kJ/mol for Zr-4, and -240 kJ/mol for Zr-2. In this work, it was problematic to conduct the assessment of thermodynamic properties because of the presence of equilibrium phases that were not observed experimentally in past work.

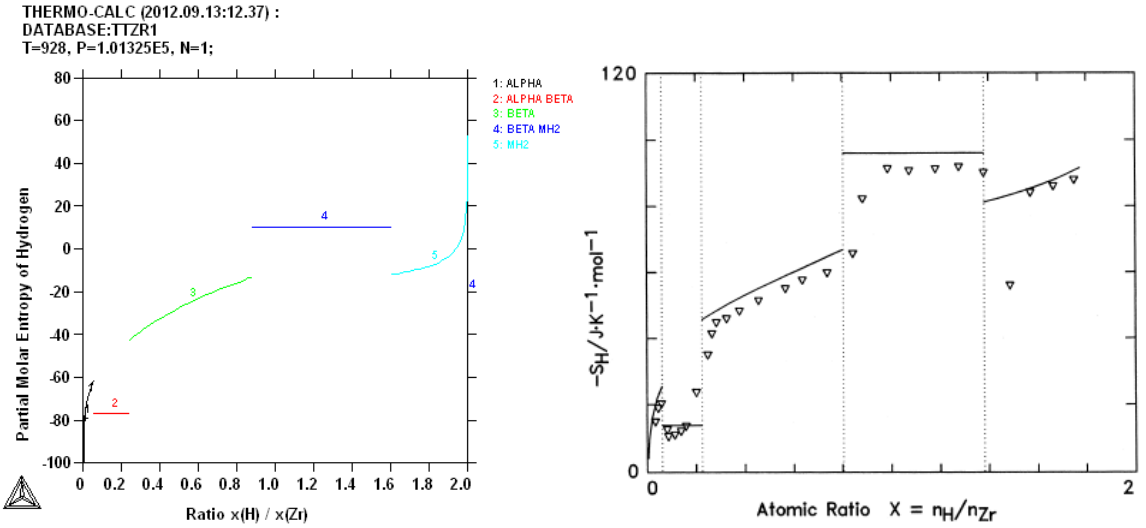

Figure 9. Partial molar entropy of hydrogen: comparison of the results of modeling (left) and experimental data [16]; black solid line –the results of thermodynamic assessment in [55] and experimental work [54].

The results for partial molar entropy of hydrogen are presented in Figure 9 below. There is a qualitative agreement between the experimental data reported in [54] and our calculations. There is a significant shift in the absolute value of ($-S_H$). However, partial molar entropy, being a second derivative of the Gibbs free energy with respect to concentration and to temperature, is notoriously unstable with respect to small errors in the input experimental information. Suffice it to say that in [23] the *values of different sign* were reported for the partial molar entropy of hydrogen of the alpha-phase. This implies only that the reassessment of the Zr-H diagram should be done to get a better agreement for nuclear Zr-bearing alloys.

2.2.2 Oxidation

Zirconium-based alloys represent the main structural materials used in light water cooled nuclear reactors (PWRs and BWRs). For these materials, the formation of a thin oxide layer with long-term kinetic stability in working reactor conditions is very important [1]. A detailed study of the diffusion of oxygen in zirconium was published by Cox, [56].

When atoms of hydrogen or oxygen occupy interstitial lattice positions between atoms of a zirconium, they form a solid solution(s). In the case of oxygen, its solubility in zirconium is quite large, about 29 at% at ambient temperature [57]. This is a consequence of the relatively large size of the octahedral sites in the hcp lattice (see Figure 1). The 29 at% of oxygen approximately corresponds to filling from 1/4 to 1/3 of interstitials in each layer of the hcp structure. One could expect that when this critical concentration of dissolved oxygen is reached, oxygen atoms and remaining interstitials will start to form some ordered structures, which results in significant reconstruction of hcp network and the onset of zirconium oxide formation. This is indeed the case [4, 58-60], and the significance of such order-disorder transformations for the reduction of hydrogen uptake will be discussed below.

There are several crystallographic modifications of ZrO_2. One is monoclinic, with the space group $P2_1/c$ and four atoms per unit cell. The lattice parameters (in Å) are a = 5.1501(2); b = 5.2077(2); and c = 5.3171(2). It does not have oxygen deficiency, i.e., the monoclinic modification is stoichiometric. This is the low temperature modification of ZrO_2 present in nature as a rare mineral, *baddeleyite*. The tetragonal modification is characterized by the space group $P4_2/nmc$, [60] and lattice parameters a = 3.6067 Å; b = 3.6067 Å; and c = 5.1758 Å, [61]. The occupancy factor for oxygen atoms in the tetragonal modification is ~0.984. This implies the tetragonal modification $ZrO_{2-\delta}$ has an oxygen deficiency of δ = 0.031. It is for this reason that stabilization of zirconia is necessary with lower valence oxides such as Y_2O_3. Finally, there is a cubic zirconia modification, FCC_C1, with space group *Fm-3m*, and lattice parameter a = 5.09 Å. The experimental and calculated Zr-O phase diagrams are presented in Figure 10 below.

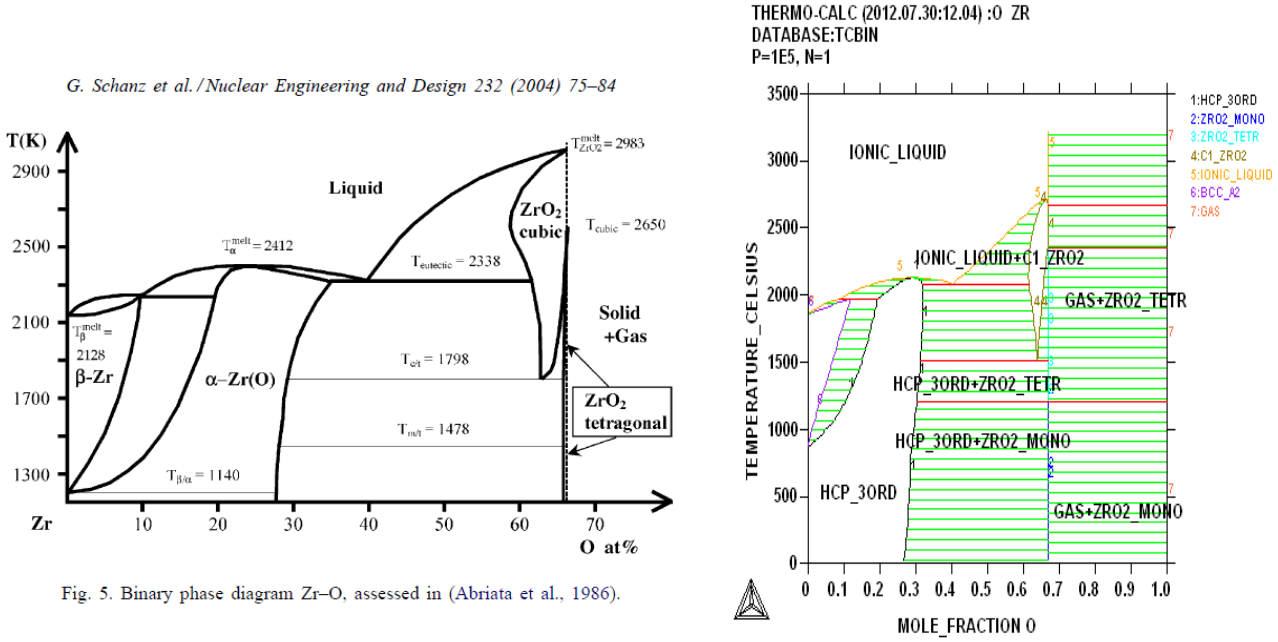

Fig. 5. Binary phase diagram Zr–O, assessed in (Abriata et al., 1986).

Figure 10. Experimental [57] and computed phase diagram Zr-O.

We computed this phase diagram with the ThermoCalc software and using the TTZR1 and TCBIN databases by ThermoTech Inc. and ThermoCalc AB, respectively. It can be seen that there is practically a one to one correspondence between the two diagrams. It should also be noted that the model of ionic liquids was used in this work to represent the behavior of the liquid phase. The results of calculation of the partial molar enthalpy of hydrogen in different phases at 650°C are presented in Figure 11.

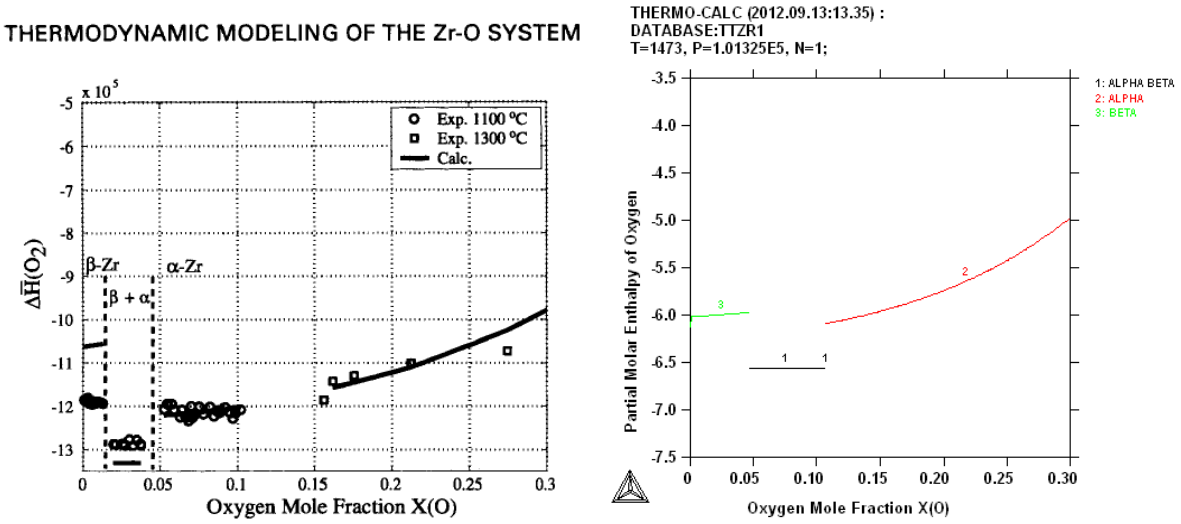

Figure 11. Partial molar enthalpy of oxygen: experimental data [62, 63], the results of assessment in [64], and the present work.

This last calculation is a good test for the physical sense of the model. Indeed, the partial molar enthalpy of the beta-phase is higher than that of the (alpha + beta) phase field. As it was demonstrated in [64], if Henry's law is followed for the beta phase, then the following relation must hold up to the point of maximum oxygen solubility (saturation):

$$\mu(O)_{\beta} = \mu(O)_{\beta/\alpha} + RT\ln\left(\frac{x(O)}{x(O)_{sat.}}\right) \tag{2-3}$$

Then, for the partial molar enthalpy of oxygen within the beta phase we will get [64]:

$$\overline{H}_{O_2,\alpha} = \frac{2\dfrac{\partial\mu(O)_{\beta/\alpha}}{\partial T}}{\partial(1/T)} = \overline{H}_{O_2,\beta/\alpha} + 2RT^2\frac{dX_O/dT}{X_O} \tag{2-4}$$

Looking at the experimental and computed phase diagram of the Zr-O system, we observe that $dX_O/dT > 0$, i.e., the partial molar enthalpy of oxygen for the (beta + alpha) region must be smaller (more negative) than that of the alpha-region, [64].

As described in the literature, two distinct oxidation periods have been observed for Zr, pre-transition and post-transition [1]. The pre-transition period is characterized by a decreasing oxidation rate and an adherent, protective film with a shiny black appearance. During the post-transition period a constant but greater oxidation rate was observed, and a less protective film formed that had a white flaky appearance. The time required to reach transition is both temperature and time dependent [1].

This change in coloration could serve a possible qualitative indicator of the undesirable transition from ZrO_2 to $Zr(OH)_4*nH_2O$. Indeed, in the precious and semi-precious stone industry a process of blackening of metallic zirconium is described, which results in beautiful shiny black coloration [65]. The raw piece is made of pure zirconium, which is then subjected to heating in a controlled oxidizing atmosphere. During this process the color changes to bronze, then to blue, then to yellow and other colors as the heat-up continues according to a prescribed thermal schedule. The initial very pure blue color is caused by the constructive interference of the light waves. As the process continues, the continuing oxidation results a second order of colors that is formed over the first, and so on. Eventually, as the oxide layer gets thicker, shiny black surface appears. These changes in coloration could be explained similar to an earlier effort by the authors to describe omni-directional coloration of metals via light scattering from textured metallic surfaces, [65].

On the other hand, hydroxides of $Zr(OH)_4*nH_2O$ are more flaky and white, [66]. This provides a possibility to measure the degree of oxidation of the underlying Zr-alloy nuclear fuel clad using a photo colorimeter.

While the phenomenon of zirconium oxidation / corrosion is very complex, the factors affecting it have been studied extensively. In particular, it is known [1] that ***impurities*** such as nitrogen, carbon, and aluminum have a pronounced deleterious effect on the corrosion resistance of Zr-2.

Heat treatment and Irradiation also affect corrosion of Zr quite substantially. Detailed synchrotron studies of second phase particle SPP precipitation and dissolution as a function of irradiation dose were reported in [67, 68]. For example, Rudling and Wikmark established that there is an optimum range for size distribution and composition of SPPs, which is correlated with the exposure conditions. They reported optimum size distributions for SPPs in the range of approximately 25-175 nm for BWR conditions. Optimum SPP Fe/Cr ratios of 0.6-1.2 and Fe/Ni ratios of 0.9-1.0 have also been found [69].

Porosity development in the oxide layers generates easy diffusion pathways for molecules during oxidation. A considerable contribution of molecular oxygen to total oxygen transport in zirconia has been observed at temperatures up to 800°C. Effective pore sizes in the nanometer range were found for pre-transition oxides on Zircaloy-2. Inward oxygen transport can be promoted by oxygen dissociating elements such as Fe-containing second phase particles. The results suggest furthermore that a proper choice of the second-phase particles composition and size distribution can lead to the formation of dense oxides, which are characterized by low oxygen and hydrogen uptake rates during oxidation.

Concerning ***oxygen diffusion via grain boundaries***, differences of several orders of magnitude between grain boundary conductivity and the conductivity inside the grains have been reported (grain boundary diffusion >> diffusion via/in grains) [70]. For oxide scales grown on Zr-based alloys at temperatures around 400°C, two crystallographic phases of zirconia have been reported: monoclinic and tetragonal. The monoclinic phase is stable at low temperatures and is, as expected, the dominating phase in the oxide scale (see the Zr-O phase diagram in Figure. 10). The tetragonal phase can also be found close to the oxide/Zr(O) interface (stabilized by the high compressive stress and grain size < 30nm) and within the oxide scale near the interface between the partially oxidized intermetallics and the bulk oxide. The oxygen vacancy concentration in zirconia, which influences the transport of oxygen through the oxide lattice, is higher in the tetragonal phase (2-3 mol %) than in the monoclinic phase (<2 mol %). The tetragonal → monoclinic phase transformation takes place with a volume increase of about 7% and has a significant impact on the corrosion behavior of Zr-based alloys [71].

In [72], it was established that the second-phase particles, or SPPs, have a high affinity for hydrogen and act as short-circuit pathways for hydrogen transport through the oxide protective layers. Hydrogen can easily diffuse through these thin oxide scales via metallic SPPs towards the metal substrate.

An interesting feature of the crystalline Zr at room temperature is an efficient repelling of interstitial atoms (H or O) from each other. The collective behavior of interstitial oxygen atoms in hcp-Zr was recently described by Ruban et al. [73]. Their calculations indicated that although interstitial oxygen atom produces just a minimal shift of the surrounding Zr atoms, it is energetically unfavorable (by about 0.5 eV) when two O atoms occupy any neighboring interstitial positions. The authors of [73] later used these atomic-scale energies in their Monte Carlo simulations of thermodynamically preferred interstitial configuration(s). We repeated these calculations and confirmed their validity. On this basis one could hypothesize that before the complete reconstruction of Zr network, oxygen might form an intermediate "checker board" configuration, and in each layer the maximal atomic concentration of oxygen would be 25 %. This is quite close to the experimental value of 29 at. %, and to the Zr_3O stoichiometric suboxide [4, 58-60]. The discrepancy in the numbers may be explained by the kinetic effects that were not taken into account in this study. For even larger oxygen concentrations, the Zr-O structure should undergo a total reconstruction, and further oxidation will eventually result in the formation of the ZrO_2.

Another interesting feature of the α–Zr structure is an impossibility of more than one atom (hydrogen or oxygen) to stay in one interstitial position. Figure 12 shows the relaxed atomic configuration for hydrogen molecule placed in a Zr octahedral interstitial; the two hydrogen atoms could not "coexist" in one octahedral interstitial position and eventually move to different interstitials. Therefore, one cannot expect hydrogen gas formation and/or hydrogen blistering as is observed at Al/Al_2O_3 interfaces; also, one cannot expect that hydrogen molecule could be positioned as a whole (as in Si and/or SiO_2) into hcp Zr crystalline lattice. At low oxygen concentrations hydrogen is unlikely to form any additional complexes except reconfiguring Zr network by forming asymmetric or broken Zr-H-Zr bonds.

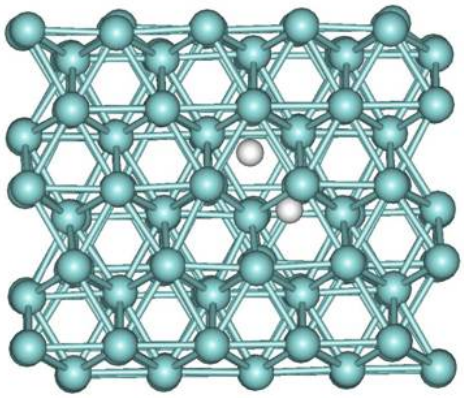

Figure 12. Relaxed configuration for two hydrogen atoms that were initially put in one octahedral interstitial (as H2 molecule). Zr atoms are shown in cyan, hydrogen – in white.

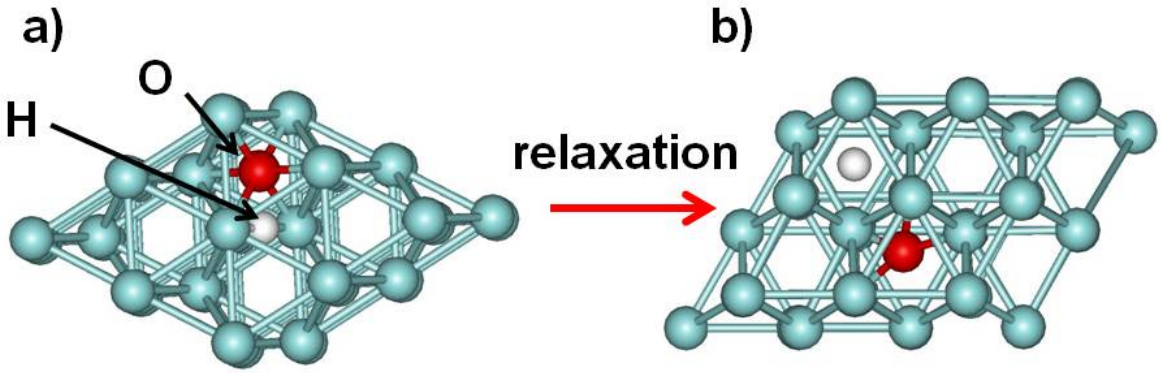

Figure 13. Relaxed configuration for H and O atoms. Initially oxygen atom was put in octahedral interstitial, and H atom – in the middle of a neighboring Zr-Zr bond. Zr atoms are shown in cyan, O – in red, H – in white.

Oxygen and hydrogen atoms also repel in the Zr hcp network. Figure 13 demonstrates how the energy relaxation of the original configuration for H and O complex actually takes place. Initially, an oxygen atom was positioned in the middle of an octahedral interstitial, while the H atom was positioned close to the neighboring Zr-Zr bonds. Relaxation forces these two atoms to move into the neighboring interstitial position instead of forming a complex within one interstitial. This is understandable; oxygen is strongly electronegative and has tendency to oxidize Zr (pull electrons away from neighboring metal atoms). Hydrogen in Zr solid solution exhibits negative valence and tends to form zirconium hydrides. Apparently, oxygen is a much stronger oxidant than hydrogen, and when oxygen is present in some interstitial, hydrogen positioned in the vicinity has no chance to find electrons at the surrounding Zr atoms. Therefore, it cannot attach itself to surrounding metal atoms and redirects itself into a neighboring interstitial that is still not occupied by oxygen.

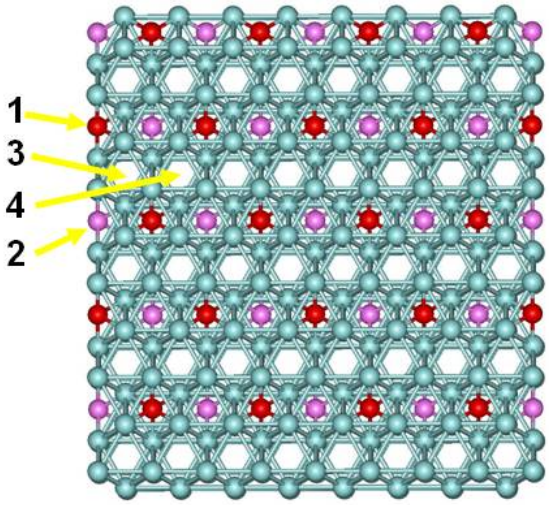

Figure 14 The "checkerboard" configuration for O atoms in octahedral interstitials. Zr atoms are shown in cyan, O in the first layer – in red, O in the second layer – in pink. Four non-equivalent groups of interstitials are indicated by numbers and yellow arrows.

Figure 2-14 illustrates the formation of the "checkerboard" configuration. In the first layer (oxygen atoms are shown in red), O is arranged in such a way that it does not occupy any two nearest neighboring interstitials. In the second layer (O atoms shown in pink), the intra-layer configuration should be similar. However, it has to shift with respect to the configuration in the first layer because we should avoid neighboring O atoms in the direction parallel to the (0001) axis of the hcp structure. In the second layer, oxygen could occupy interstitials of the type 3 and 4 with the same probability. In the third layer, several possibilities to arrange O atoms in checkerboard structure become available again, and so on. An important conclusion that comes from such a construction is that after several layers of octahedral interstitial are occupies with oxygen in concentration close to the critical (25 at. %), all the direct paths through hcp structure oriented along the (0001) direction for hydrogen atoms will be blocked by shifted checker board oxygen layers, and in order to migrate in the structure, any additional hydrogen atom will need to migrate not only in the (0001) direction but also laterally within the hcp Zr layers.

2.2.3 Suboxides of Zirconium

Suboxides of transition metals such as titanium, zirconium, vanadium, etc., were discovered in the early 1960s [4, 58-60]. At temperatures between (about) 300°C and 900°C various ordered phases have been reported [5]. Octahedral interstitial ordering of oxygen increases the microhardness [58] and embrittlement [74], and therefore, promotes stress corrosion cracking. However, as it will be demonstrated later, oxygen can be very beneficial for reducing the hydrogen uptake under certain conditions, [71].

Order-disorder transitions in the zirconium – oxygen system were studied using heat capacity measurement for alloys with O/Zr ratios of 0.16 and 0.24 at 200°C – 700°C [75]; and alloys with O/Zr ratios of 0.0, 0.10, 0.13, and 0.24, at 52°C – 632°C. In particular, a high degree of long-range ordering was achieved in samples that were cooled from 350°C to 250°C, during a period of about one month. This clearly indicates that a high mobility of oxygen is observed in the α–Zr matrix even at such modest temperatures [61]. These temperatures are directly relevant to the conditions of the used nuclear fuel storage and so is the formation of sub-oxides.

Inside the metal, oxygen is randomly distributed in octahedral interstitial positions up to a concentration of 0.33 mole fraction of O. Yilmazbayhan et al. [76] identified the formation of ordered suboxides (Zr_3O) at the oxide / α–Zr interface underneath the oxide and ahead of the oxidation front, by using microbeam synchrotron radiation diffraction. Oxygen uptake has a hardening effect on the Zr matrix, this effect is actually used in one of the novel Zr-Nb-O nuclear alloys, "M5™". Cox [5] established that at temperatures around 400°C, less than 10% of the reacting oxygen is expected to dissolve into the metal substrate. He proved experimentally that preferential dissolution of oxygen, from the already formed oxide layer, takes place along the grain boundaries of Zr accompanied by the formation of arrays of pores in the oxygen-depleted grain boundaries (oxide) just above the metal substrate. These defective grain boundaries are possible open porosity development sites.

A clear correlation was found between oxide-metal interfacial microstructure and protective nature of the oxide (when interfacial structure is present, oxide is protective, when it is not present, oxide is not protective) [10-12, and 76].

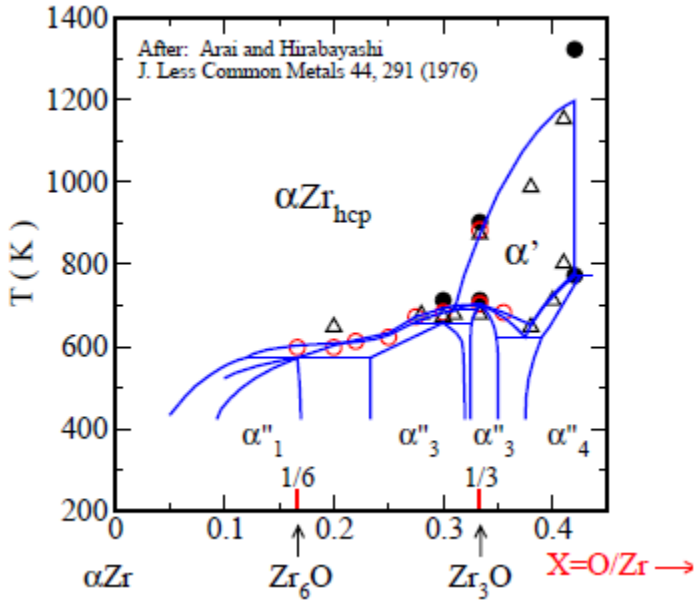

Figure 15. Experimentally constructed isothermal cross-section for the Zr-O-H phase diagram at 700°C, [61 and 75].

The structure of the oxide–metal interface is of great interest to understanding the mechanism of oxide growth and the differences between the protective and non-protective oxides. As it was demonstrated in [10-12], the protective alloys always exhibit extra peaks in the diffraction scans obtained near the oxide–metal interface region. These peaks have been associated with two different phases found in that region in the protective oxides:

(i) A highly oriented tetragonal phase that has been hypothesized to be a crystallographic precursor of the monoclinic phase observed in the bulk of the oxide.

(ii) *The formation of the sub-oxide phase Zr_3O.* This phase has also been seen at the oxide–metal interface by various researchers in oxides formed in Zr alloys at low temperature [77-82]. In particular, the diffraction pattern from synchrotron radiation shows strong Zr_3O peaks in a two to three micron region next to the oxide–metal interface corrosion.

Summarizing these results, characteristic differences seem to exist in the oxide–metal interface regions of protective and non-protective oxides. In particular, the presence of two interfacial oxide phases, a highly oriented tetragonal phase and a sub-oxide phase was associated with protective behavior uniform is deemed critical for the reduction in hydrogen pick-up. These results stimulated further first-principles calculations aimed at understanding the atomic mechanisms of such protection. These results are presented in the next Section.

2.2.4 Interstitial Oxygen and Hydrogen Solid Solutions

To understand the migration mechanisms of hydrogen in zirconium suboxides, migration barriers for oxygen and hydrogen in interstitial solid solutions were calculated using the nudged elastic band approach [83]. It was established that, unlike in pure Zr, inside the zirconium suboxide lattice the migration barrier for moving oxygen atom from one octahedral interstitial to another is very high (>2 eV). In turn, this implies that oxygen atoms are not mobile at moderate temperatures (below 600 – 800^{o}C). A high migration barrier for oxygen in a suboxide is not surprising; it follows immediately from the simple geometric arguments (comparison between Zr-O and Zr-Zr bond lengths). Indeed, while an oxygen atom is put in some octahedral interstitial, it will stay there before either the temperature increases or the hcp Zr network significantly changes due to increase of oxygen atoms concentration above the critical value that hcp network can still tolerate. From the thermodynamics point of view, the checkerboard oxygen ordering (Figure 14) is energetically favorable. However, if because of kinetic reasons two oxygen atoms will become neighbors, their rearrangement towards an energetically favorable configuration will develop on a very slow time scale. Therefore, because of kinetics we could expect checkerboard distortions in the "real" suboxide systems.

Apparently, ordering of low-mobile oxygen atoms in Zr_3O changes the dynamics of hydrogen propagation through this class of materials. Assuming that the hydrogen concentration gradient is directed along the (0001) axis, the following two modifications of the original hcp Zr matrix by oxygen are realized. First, the oxygen checkerboard arrangement shuts down "vertical" channels for hydrogen propagation along the (0001) axis. Moving along each of these, originally preferable migration paths, hydrogen will interact inevitably with oxygen atoms (this interaction is repulsive) positioned along this path. It means that the trajectory will be different than a straight line, i.e., it will become longer by necessity. Secondly, migration barriers for hydrogen between two octahedral interstitials increase when an oxygen atom is present in the neighboring interstitial. In the absence of oxygen, the migration barrier between two interstitials was determined to be about 0.6 eV, in agreement with earlier calculations. On the other hand, when oxygen is present in the neighboring interstitial, this barrier increases to 0.9 eV. Therefore, in addition to increasing the length of hydrogen migration paths, a presence of oxygen increases hydrogen migration barriers. Both factors are unfavorable for hydrogen migration and it explains why hydrogen will propagate slower in Zr_3O than in pure zirconium.

Another interesting observation is that in the vicinity of oxygen atoms trapped in octahedral interstitials, hydrogen might migrate by another mechanism, namely through the middle of Zr-Zr bonds. In such a case, H atom distorts the Zr-Zr bond, forms the asymmetric Zr-H-Zr configuration, and eventually may break the original Zr-Zr bond. This process might be considered a precursor to the formation of stoichiometric hydride. Bond breaking will modify the hydrogen migration process even further, in favor of its' slowing down.

2.2.5 CONCLUSIONS AND RECOMMENDATIONS

In the first part of this report we presented the results of computational thermodynamics and first-principles atomistic studies of the processes of hydrogen uptake and corrosion of zirconium and its alloys, including the detailed calculations of the Gibbs free energy of the competing phases in the Zr-H system at different temperatures (see Appendix). It was established that for pure Zr, alloys Zr-2 and Zr-4 the differences in hydrogen uptake could not be explained using thermodynamic arguments as the hydrogen solvi and hydrogen saturation points were practically the same in all three materials: temperature of hydride dissolution 550°C and ~0.056 hydrogen molar fraction. A conclusion was made that to understand the mechanisms of reduced hydrogen uptake rates, it was necessary to understand the kinetics of the hydrogen diffusion process and the role of the Zr_3O suboxide forming underneath the layer of ZrO_2 at the depth of about 2 to 3 microns. This work was done using the first principles calculations, which demonstrated that the formation of Zr_3O seems to be critical for reducing hydrogen diffusion of bulk Zr alloy. In turn, this implies that the cladding temperature in storage should not exceed 360°C, when the disordering reaction takes place accompanied by the formation of the disordered Zr-O solid solution. This conclusion is based upon the detailed analysis of the corresponding portion of the Zr-O phase diagram and our first-principles atomistic calculations.

These results have direct application to phase-field simulations of the zirconium hydride microstructure evolution and reorientation (data on the driving forces for hydride formation in the form of a look-up table).

More accurate modeling by kinetic Monte Carlo simulations of these order-disorder transformations and their role in slowing down the hydrogen uptake in nuclear zirconium alloys would have important implications for drying and, possibly even, alloy development.

Also, a detailed work on the development of self-consistent phase diagram region corresponding to these transformations should be conducted on the base of data generated from first-principles calculations on the temperature dependence of the free energy of the suboxide formation and not the semi-empirical Miedema rules, [64].

2.2.6 REFERENCES

1. L. Whitmarsh, Review Of Zircaloy-2 and Zircaloy-4 Properties Relevant to N.S. Savannah Reactor Design, ORNL-3281, Oak Ridge National Laboratory (1962)
2. G.P. Sabol in: Zirconium in the Nuclear Industry: 14th International Symposium, **2004**, Stockholm, Sweden, ASTM International, STP 1467, p.3.
3. K.L. Murty, I. C. *Progress in Nuclear Energy,* **2006**, *48*, p. 325.
4. I.I. Kornilov, V.V. Glazova (Vavilova), and E.M. Kenina, Reports of the USSR Academy of Sciences, vol.169, p.343 (1966)
5. B. Cox, *Journal of Nuclear Materials, vol. 336*, p. 331 (2005).
6. G.E. Zima, A Review of the Properties of Zircaloy-2, HW-60908, (October 14, 1959)
7. B. Lustman and F. Kerze, The Metallurgy of Zirconium, McGraw-Hill, New York (1955)
8. D. Setoyama, *Journal of Nuclear Materials, vol. 344*, p. 291 (2005).
9. D. Arias; T. Palacios; C. Turillo, *Journal of Nuclear Materials, vol.148*, p.227 (1987).
10. A. Motta, A. Yilmazbayhan, M. Gomes da Silva, R. J. Comstock, G. Was, J. Busby, E. Gartner, Q. Peng, Y.H. Jeong, and J. Y. Park, "Zirconium Alloys for Supercritical Water Reactor Applications: Challenges and Possibilities," *Journal of Nuclear Materials* 371 (2007) 61-75.

11. A. Yilmazbayhan, Microstructural Basis, of Uniform Corrosion in Zr Alloys, Ph.D. Thesis in Nuclear Engineering, Pennsylvania State University (2004)

12. A. Motta, A. Yilmazbayhan, R.J. Comstock, J. Partezana, G.P. Sabol, Z. Cai and B. Lai, Microstructure and Growth Mechanism of Oxide Layers Formed in Zr Alloys Studied with Micro-Beam Synchrotron Radiation, *Journal of ASTM International,* vol.2, Paper # JAI 12375 (2005)

13. Klara Anghel, Modified Oxygen and Hydrogen Transport in Zr-Based Oxides, Doctoral Thesis, Division of Corrosion Science, Department of Materials Science and Engineering Royal Institute of Technology (KTH) Stockholm, Sweden (2006).

14. Benjamin P. Burton, Axel Van der Valle, Harold T. Stokes, First Principles Phase Diagram Calculations for the Octahedral-Interstitial System ZrO_x, $0 < X < 0.5$; NIST preprint, July 11 (2011)

15. M.C. Payne, M.P. Teter, D.C. Allan, T.A. Arias, J.D. Joannopoulos, *Rev. Mod. Phys*., vol. *64*, 1045-1097 (1992).

16. J.P. Perdew, K. Burke, M. Ernzerhof, *Phys. Rev. Lett*., vol.*77*, 3865-3868 (1996).

17. P.E. Blöchl, *Phys. Rev. B*, vol.*50*, 17953-17979 (1994).

18. G. Kresse, J. Joubert, *Phys. Rev. B*, *59*, 1758-1775 (1999).

19. G. Kresse, J. Hafner, *Phys. Rev. B,* vol.*48*, 13115-13118 (1993); also see G. Kresse, J. Furthmüller, *Phys. Rev. B*, vol.*54*, 11169-11186 (1996).

20. D.J. Chadi, M.L. Cohen, *Phys. Rev. B* vol.*8*, 5747-5753 (1973).

21. H. Jonsson, G. Mills, K.W. Jacobsen, *Classical and Quantum Dynamics in Condensed Phase Systems*; World Scientific, Singapore, p 385 (1998)

22. M. Hillert: Phase Equilibria, Phase Diagrams, and Phase Transformations, Cambridge University Press, Cambridge, UK (2007)

23. H.L. Lukas, S.G. Fries, and Bo Sundman, Computational Thermodynamics (The CALPHAD Method), Cambridge University Press, Cambridge (2007)

24. N. Saunders and A.P. Miodownik, CALPHAD – Calculation of Phase Diagrams. A Comprehensive Guide, Pergamon, London (1998)

25. Zi-Kui Liu, First-Principles calculations and CALPHAD Modeling of Thermodynamics, Journal of Phase equilibria and Diffusion, published online 03 September (2009)

26. L.J. Siefken, Preliminary Design Report for Modeling of Hydrogen Uptake in Fuel Rod Cladding during Severe Accidents, INEEL, September 14 (1998)

27. A. Sawatsky, the Diffusion and Solubility of Hydrogen in the Alpha Phase of Zircaloy-2, *Journal of Nuclear Materials*, vo.2, No.1, pp.62-68 (1960)

28. G. Ostberg, Determination of Hydride Solubility in Alpha Phase Zirconium, Zircaloy-2, and Zircaloy-4, *Journal of Nuclear Materials,* vol.5, No.2, pp.208-215 (1962)

29. J.J. Kearns, Terminal Solubility and Partitioning of Hydrogen in the Alpha Phase of Zirconium, Zircaloy-2, and Zircaloy-4, *Journal of Nuclear Materials,* vol.22, pp.292-303 (1967)

30. S. Yamanaka, M. Miyake, M. Katsura, Study on the Hydrogen Solubility in Zirconium Alloys, *Journal of Nuclear Materials,* vol.247, pp.315-321 (1997)

31. O. Zanellato, M. Preuss, J.-Y. Buffiere, F. Ribeiro, A. Stewer, J. Desquines, J. Andrieux, B. Krebs, Synchrotron Diffraction Study of Dissolution and Precipitation Kinetics of Hydrides in Zircaloy-4, *Journal of Nuclear Materials,* vo. 420, pp.537-547 (2012)

32. J. Xu, and S.-Q Shi, Investigation of Mechanical Properties of ε-Zr hydride Using Micro- and Nano-Indentation Techniques, *Journal of Nuclear Materials,* vol.327, pp.165-170 (2004)

33. D. G. Westlake, The Habit Planes of Zirconium Hydride in Zirconium and Zircaloy, *Journal of Nuclear Materials,* vol.26, pp.208-216 (1968)

34. V.S. Arunachalam, B. Lenthinen, and G. Ostberg, The Orientation of Zirconium Hydride on Grain Boundaries in Zircaloy-2, *Journal of Nuclear Materials*, vol.21, pp.241-248 (1967)

35. J. Blomquist, J. Oloffson, A.-M. Alvarevol.z, C. Bjerken, Structure and Thermodynamic Properties of Zirconium Hydrides from First Principles, Preprint, University of Malme, Sweden (2010)

36. W. Zhu, R. Wang, G. Shu, P. Wu, H. Ziao, First-Principles Study of Different Polymorphs of Crystalline Zirconium Hydride, *Journal of Physical Chemistry C,* vol.114 (50), pp.22361-22368 (December 23, 2010)

37. Ma, X. Q., Shi, S. Q. et al., "Effect of Applied Load on Nucleation and Growth of gamma-Hydrides in Zirconium," *Comput. Mater. Sci.*, Vol. 23, 2002, p. 283.

38. Domizzi, G., Enrique, R. A. et al., "Blister Growth in Zirconium Alloys: Experimentation and Modeling," *J. Nucl. Mater.*, Vol. 229, 1996, p. 36

39. Carpenter, G. J. C., "The precipitation of Gamma-Zirconium Hydride in Zirconium," *Acta Metall.* Vol. 26, 1978, p. 1225

40. Bradbrook, J. S., Lorimer, G. W. et al., "The Precipitation of Zirconium Hydride in Zirconium and Zircaloy-2," *J. Nucl. Mater.*, Vol. 42, 1972, p. 1

41. Kearns, J. J., "Terminal Solubility and Partitioning of Hydrogen in the Alpha Phase of Zirconium, Zircaloy-2 and Zircaloy-4," *J. Nucl. Mater.*, Vol. 22, 1967, p. 292

42. Bailey, J. E., "Electron Microscope Observations on the Precipitation of Zirconium Hydride in Zirconium," *Acta Metall.*, Vol. 11, 1963, p. 267

43. Z. Zhao, M. Blat-Yrieix, J.-P. Morniroli, A. Legris, L. Thuinet, Y. Kihn, A. Ambard, and

44. L. Legras, Characterization of Zirconium Hydrides and Phase Field Approach to Meso-scopic Scale Modeling of Their Precipitation, *Journal of ASTM International*, Vol. 5, No. 3 Paper ID JAI101161

45. X.Q. Ma, S.Q. Shi, C.H. Woo, and L.Q. Chen, The phase field model for hydrogen diffusion and c-hydride precipitation in zirconium under non-uniformly applied stress, *Mechanics of Materials,* vol. 38, pp. 3–10 (2006)

46. Z. Zhao, M. Blat-Yrieix, J.-P. Morniroli, A. Legris, L. Thuinet, Y. Kihn, A. Ambard, L. Legras, Characterization of Zirconium Hydrides and Phase Field Approach to a Meso-scopic-Scale Modeling of Their Precipitation*, Journal of ASTM International*, vol. 5, Issue 3 (March 2008)

47. James H. Saling and Audeen W. Fentiman, Radioactive Waste Management, 2nd edition, Taylor and Francis, New York (2001)

48. C. -S. Zhang; B. Li; P.R. Norton, *Journal of Alloys and Compounds,* vol.*231*, p. 354 (1995)

49. E. Zuzek, J.P. Abriata, A. San Martin, and F.D. Manchester, H-Zr (Hydrogen-Zirconium), Binary Alloy Phase Diagrams, II Ed., Ed. T.B. Massalski, Vol. 2, p 2078-2080 (1990)

50. *Van der Sande, J.B. and A.L. Bement. "An Investigation of Second Phase* Particles in Zircaloy-4 Alloy", *Journal of Nuclear Materials*, vol. 52. pp. 115-134 (1974)

51. *Krasevec, V, "Transmission Electron Microscopy Study of Second* Phase Particles in Zircaloy- 2," *Journal of Nuclear Materials*, vol. 98, p. 235 (1981)

52. P. Mukhopadhyay and V. Raman, Metallography, vol.11 p.481 (1978)

53. N.(Rao)V. Bangaru, An investigation of the microstructures of heat-treated Zircaloy-4, *Journal of Nuclear Materials*, vol. 131, issues 2–3, pp.280–290 (1985)

54. Erwin, K. T., Delaire, O., Motta, A. T., Birtcher, R. C., Chu, Y., and Mancini, D., "Observation of Second Phase Particles in bulk Zirconium Alloys Using Synchrotron Radiation," *Journal of Nuclear Materials*, 294, (2001) 299-304.

55. P. Dantser, W. Luo, T.B. Flanagan, J.D. Clewley, Metallurgical Transactions A, vol.24, p.1471 (1993)

56. E. Konigsberger, G. Eriksson, and W.A. Oates, Optimization of the Thermodynamic Properties of the Ti-H and Zr-H Systems, Journal of Alloys and Compounds, vol. 299, pp.148-152 (2000)

57. B. Cox; J.P. Pemsler, *Journal of Nuclear Materials,* vol.*28*, p. 73 (1968)

58. J.P. Abriata, J. Garces, R. Versaci, The O–Zr (Oxygen– Zirconium) System, *Bull. Alloy Phase Diagrams,* vol. 7 (2), p.116 (1986); also see D. Setoyama and S. Yamanaka, Phase Diagram of Zr-O-H ternary system, *J. Alloys Compd*., vol. 370, p 144-148 (2004)

59. A. Dubertret and P. Lehr, *Compt. Rendus Acad. Sc. Paris*, vol. 262, p. 1147 (1966).

60. L.M. Kovba, E.M. Kenina, I.I.Kornilov, and V.V. Glazova, Investigation into Ordered Structures of Zr_6O and Zr_3O Suboxides, Reports of the USSR Academy of Sciences, vol. 180, issue 2, p. 360 (1968)

61. I.I. Kornilov and V.V. Glazova, Formation Of Ti_6O and Ti_3O Compounds In Titanium-Oxygen System, Reports of the USSR Academy of Sciences, vol. 150, iss. 2, p.313 (1963)

62. B.P. Burton, A. van de Walle, H.T. Stokes, First Principles Phase Diagram Calculations for the Octahedral-Interstitial System $\underline{ZrO_x}$, $0 < x < 1/2$, *J. of the Physical Society of Japan,* vol. 81., iss. 1, art. 014004 (January 2012)

63. G. Boreau and P. Gerdanian, High Temperature Thermodynamics of Solutions of Oxygen in Zirconium and Hafnium, *J. Phys. Chem. Solids*, vol.45, pp.141-145 (1984)

64. G. Boreau and P. Gerdanian, Use of Tian-Valve Micro-Calorimeter at 1300°C for Direct Measurement of Partial Molar Enthalpy of Oxygen in the Metal-Oxygen Systems, *Can. Metall. Q.,* vol.13 pp.339-343 (1974)

65. R. Arroyave, L. Kauffman, and T.W. Eagar, Thermodynamic Modeling of the Zr-O System, *Calphad,* vo.26,, no.1, pp. 95-118 (2002)

66. http://www.titaniumstyle.com/black-zirconium-ring.html

67. Chuanyong Huang, Zilong Tang, Zhongtai Zhang, Differences between Zirconium Hydroxide ($Zr(OH)_4 \cdot n$H2O) and Hydrous Zirconia ($ZrO_2 \cdot nH_2O$), *Journal of the American Ceramic Society,* vol. 84, iss. 7, pp. 1637–1638 (July 2001)

68. P. Vizcaíno, A. D. Banchik, J. P. Abriata. "Synchrotron x-ray Diffraction Evidences of the Amorphization / Dissolution of the Second Phase Particles (SPPs) in Neutron Irradiated Zircaloy-4", *Materials Letters*, vol.62, pp. 491–493 (2008)

69. P. Vizcaíno , A. D. Banchik, J. P. Abriata. "Hydrogen in Zircaloy-4: Effects of the Neutron Irradiation on the Hydride Formation", *Journal of Materials Science*, vol. 42, pp.6633-6637 (2007)

70. P. Rudling; G. Wikmark, *Journal of Nuclear Materials*, vol. 265, p.44 (1999)

71. K. R. Lawless, *Rep. Prog. Phys.* vol. *37*, p. 231 (1974)

72. A. Yilmazbayhan, A.T. Motta, R.J. Comstock, G.P. Sabol, B. Lai,Z.H. Cai, Structure of zirconium alloy oxides formed in pure water studied with synchrotron radiation and optical microscopy: relation to corrosion rate, *Journal of Nuclear Materials*, vol.324, p.6 (2004)

73. C. Andrieu; S. Ravel; G. Ducros; C. Lemaignan, *Journal of Nuclear Materials*, *347*, p. 12 (2005)

74. A.V. Ruban, V.I. Baikov, B. Johansson, et al., Oxygen and nitrogen interstitial ordering in hcp Ti, Zr, and Hf: An *ab-initio* study, Physical Review B, vol.82, iss.13, art.134110 (October 14, 2010)

75. A. W. Cronenberg, M. S. El-Genk *J. Nucl. Materials* 78, 390 (1978).

76. T. Arai and M. Hirabayashi, Journal of the Less-Common Metals, vol. 44, p.291 (1976)

77. A.Yilmazbayhan, E. Breval, A.T. Motta, R.J. Comstock, *Journal of Nuclear Materials,* vol. 349, p.265 (2006).

78. I.G. Ritchie, A. Atrens, *J. Nucl. Mater*. 67 (1977) 254.

79. Yoshitaka Nishino, A.R. Krauss, Yuping Lin, D.M. Gruen, *J. Nucl. Mater.,* vol.228, p. 346 (1996).

80. C. Morant, J.M. Sanz, L. Galan, L. Soriano, F. Rueda, *Vacuum* 39 (1989) 860.

81. M.C. Deibert, B.P. Thiesen, R. Kahraman, *Appl. Surf. Sci*., 35 (1989) 302.

82. C.O. De Gonzalez, E.A. Garcia, Appl. *Surf. Sci.,* vol.44, p.211 (1990).

83. T. Ericsson, G. Ostberg, B. Lehtinen, *J. Nucl. Mater*., vol.25, p.322 (1968).

84. G. Mills and H. Jonsson, *Phys. Rev. Letts,* vol.72, p.1124 (1994)

APPENDIX. THERMODYNAMIC PROPERTIES OF DIFFERENT PHASES

IN THE Zr-H SYSTEM AT DIFFERENT TEMPERATURES

Table A1 Gibbs thermodynamic potentials of different phases in the Zr-H system at 300°C (in J/mole)

X(H)	GMR(GAS)	GMR(IONIC_LIQ)	GMR(BCC_A2)	GMR(C1_FCC)	GMR(HCP_ZR)	GMR(ZRH2_EPS)
0.99975	94.42769	399892.2	11947.52	-28551.1	-11064.1	-30276.6
0.994546	2100.338	397727.4	11947.52	-28551.1	-11064.1	-30276.6
0.969546	11852.58	387562.9	11947.52	-28551.1	-11064.1	-30276.6
0.944545	21663.18	377515.2	11947.52	-28551.1	-11064.1	-30276.6
0.919546	31503.19	367526.2	11947.52	-28551.1	-11064.1	-30276.6
0.894545	41363.64	357578.1	11947.52	-28551.1	-11064.1	-30276.6
0.869546	51240.01	347661.9	11947.52	-28551.1	-11064.1	-30276.6
0.844546	61129.58	337772	11947.52	-28551.1	-11064.1	-30276.6
0.819545	71030.52	327905	11947.52	-28551.1	-11064.1	-30276.6
0.794546	80941.56	318058.1	11947.52	-28551.1	-11064.1	-30276.6
0.769545	90861.74	308229.4	11947.52	-28551.1	-11064.1	-30276.6
0.746623	99964.98	299232.3	9739.014	-28551.1	-11064.1	-30276.6
0.744546	100790.3	298417.6	8485.626	-28551.1	-11064.1	-30276.6
0.721623	109900.8	289434.9	-2427.43	-28551.1	-11064.1	-30276.6
0.719546	110726.8	288621.5	-3208.64	-28551.1	-11064.1	-30276.6
0.696623	119844	279652.4	-10156.3	-28551.1	-11064.1	-30276.6
0.694545	120670.6	278840.1	-10656.6	-28551.1	-11064.1	-30276.6
0.671623	129794.2	269883.9	-15084.1	-28551.1	-11064.1	-30276.6
0.669546	130621.4	269072.8	-15399.6	-28551.1	-11064.1	-30276.6
0.664347	132691.4	267043.5	-16136.1	-28764.1	-11064.1	-30262.2
0.66431	132706.1	267029.1	-16141.1	-28766.9	-11064.1	-30261.5
0.646623	139751.3	260129	-18143.8	-29446.4	-11064.1	-29582.8
0.644545	140579	259319	-18334.2	-29470.5	-11064.1	-29485.6
0.639347	142650.4	257292.4	-18774.2	-29493.4	-11064.1	-29235.3
0.63931	142665	257278	-18777.2	-29493.4	-11064.1	-29233.5
0.621623	149714.8	250387.1	-19927.1	-29240.6	-11064.1	-28332.8
0.619546	150543	249578.1	-20031.1	-29183.2	-11064.1	-28223.8
0.614347	152615.8	247554.2	-20265.9	-29018.1	-11064.1	-27949.3
0.61431	152630.5	247539.9	-20267.4	-29016.8	-11064.1	-27947.3
0.596623	159684.7	240657.8	-20823.6	-28261.1	-11064.1	-26999
0.596623	159684.7	240657.8	-20823.6	-28261.1	-11064.1	-26999
0.594546	160513.4	239849.9	-20867.1	-28155.8	-11064.1	-26886.6
0.589347	162587.5	237828.6	-20958	-27879.4	-11064.1	-26604.9
0.58931	162602.2	237814.3	-20958.6	-27877.4	-11064.1	-26602.9
0.571623	169660.7	230941	-21096.7	-26820.7	-11064.1	-25639.7
0.569545	170490	230134.1	-21097.5	-26686.7	-11064.1	-25526.3
0.564347	172565.3	228115.3	-21086.7	-26343.9	-11064.1	-25242.4
0.56431	172580	228101	-21086.6	-26341.4	-11064.1	-25240.4
0.546623	179642.9	221236.3	-20928.3	-25108.1	-11064.1	-24273.4
0.544546	180472.7	220430.4	-20898.7	-24957.7	-11064.1	-24159.8
0.539347	182549.2	218414.1	-20815.6	-24577.3	-11064.1	-23875.6
0.53931	182563.9	218399.8	-20815	-24574.5	-11064.1	-23873.6
0.521623	189631	211543.6	-20445.7	-23245.4	-11064.1	-22906.8
0.519545	190461.3	210738.7	-20394.5	-23086.6	-11064.1	-22793.3
0.514347	192539.1	208724.9	-20259.9	-22687.5	-11064.1	-22509.4
0.51431	192553.8	208710.7	-20258.9	-22684.6	-11064.1	-22507.3
0.496623	199625.2	201862.9	-19739.5	-21313.3	-11160.1	-21542
0.494546	200455.9	201059	-19673	-21151.4	-11194.2	-21428.6
0.494546	200455.9	201059	-19673	-21151.4	-11194.2	-21428.6
0.489347	202534.9	199047.7	-19501.8	-20746.1	-11250.2	-21145.1
0.48931	202549.7	199033.4	-19500.6	-20743.3	-11250.5	-21143.1
0.478571	206845.2	194880.2	-19128.1	-19906	-11295.7	-20557.7
0.471623	209625.2	192194	-18874.8	-19365.4	-11294.7	-20179.1
0.469546	210456.5	191391.1	-18797.4	-19204	-11291.1	-20066
0.464347	212536.8	189382.3	-18600.5	-18800.9	-11276.2	-19782.8
0.46431	212551.5	189368.1	-18599.1	-18798.1	-11276.1	-19780.8
0.453571	216849.6	185220	-18179	-17969.7	-11223.3	-19195.9
0.446623	219631.3	182537.2	-17898.7	-17437.3	-11175.9	-18817.6
0.444545	220463	181735.3	-17813.8	-17278.8	-11160	-18704.5
0.439347	222544.6	179728.9	-17598.9	-16883.5	-11117	-18421.4
0.43931	222559.3	179714.7	-17597.4	-16880.7	-11116.7	-18419.4
0.428571	226860	175571.8	-17144.4	-16071	-11014.4	-17834.6
0.421623	229643.4	172892.4	-16845.5	-15552.5	-10939.7	-17456.2
0.419545	230475.6	172091.5	-16755.4	-15398.3	-10916.2	-17343.1
0.414347	232558.4	170087.7	-16528.3	-15014.3	-10855.1	-17059.9
0.41431	232573.2	170073.5	-16526.7	-15011.6	-10854.6	-17057.9
0.403571	236876.5	165935.8	-16051.5	-14227	-10718.7	-16472.6
0.396623	239661.6	163259.8	-15740.2	-13725.7	-10624.3	-16093.8
0.394546	240494.3	162459.9	-15646.7	-13576.8	-10595.2	-15980.5
0.389347	242578.4	160458.7	-15411.6	-13206.3	-10520.5	-15696.8
0.38931	242593.2	160444.5	-15409.9	-13203.7	-10520	-15694.8
0.378571	246899.2	156312.2	-14920.4	-12448	-10358.1	-15108.6
0.371623	249686	153639.6	-14601.3	-11965.9	-10248.1	-14728.9

0.369546	250519.3	152840.8	-14505.5	-11822.9	-10214.5	-14615.3
0.364347	252604.7	150842.2	-14265.5	-11467.1	-10128.9	-14331
0.36431	252619.5	150828	-14263.8	-11464.6	-10128.3	-14329
0.353571	256928.2	146701.2	-13765.6	-10739.8	-9945	-13741.1
0.346623	259716.8	144032.2	-13441.9	-10278	-9821.99	-13360.3
0.344546	260550.6	143234.5	-13345	-10141.1	-9784.57	-13246.4
0.339347	262637.3	141238.6	-13102.1	-9800.61	-9689.64	-12961.1
0.33931	262652.2	141224.4	-13100.4	-9798.21	-9688.96	-12959.1
0.328571	266963.7	137103.3	-12597.7	-9105.08	-9487.23	-12369
0.328571	266963.7	137103.3	-12597.7	-9105.08	-9487.23	-12369
0.321623	269754.2	134438	-12271.8	-8663.86	-9352.81	-11986.6
0.319545	270588.6	133641.3	-12174.3	-8533.06	-9312.04	-11872.2
0.314347	272676.7	131648.2	-11930.3	-8207.95	-9208.88	-11585.7
0.31431	272691.5	131634.1	-11928.5	-8205.66	-9208.14	-11583.6
0.303571	277006	127518.9	-11424.1	-7544.16	-8989.96	-10990.8
0.296623	279798.4	124857.4	-11097.7	-7123.28	-8845.25	-10606.5
0.294545	280633.3	124061.9	-11000.2	-6998.53	-8801.45	-10491.4
0.289347	282722.9	122071.8	-10756	-6688.53	-8690.81	-10203.4
0.28931	282737.8	122057.7	-10754.3	-6686.34	-8690.02	-10201.3
0.278571	287055.3	117948.5	-10250.3	-6055.74	-8456.75	-9605.1
0.271623	289849.7	115291.1	-9924.42	-5654.62	-8302.52	-9218.45
0.269546	290685.3	114496.9	-9827.05	-5535.74	-8255.91	-9102.71
0.264347	292776.4	112509.8	-9583.54	-5240.34	-8138.29	-8812.81
0.26431	292791.2	112495.7	-9581.81	-5238.25	-8137.45	-8810.75
0.253571	297112	108393	-9079.4	-4637.4	-7890.02	-8210.53
0.246623	299908.6	105739.9	-8754.81	-4255.2	-7726.77	-7821.13
0.244546	300744.8	104946.9	-8657.84	-4141.92	-7677.49	-7704.55
0.239347	302837.6	102963.1	-8415.37	-3860.43	-7553.21	-7412.49
0.23931	302852.4	102949	-8413.65	-3858.45	-7552.33	-7410.42
0.228571	307176.7	98853.27	-7913.56	-3285.82	-7291.3	-6805.51
0.221623	309975.5	96204.72	-7590.54	-2921.49	-7119.34	-6412.91
0.219546	310812.4	95413.13	-7494.06	-2813.5	-7067.46	-6295.35
0.214347	312906.9	93432.81	-7252.8	-2545.1	-6936.71	-6000.77
0.21431	312921.8	93418.77	-7251.09	-2543.21	-6935.78	-5998.68
0.203571	317249.7	89330.43	-6753.52	-1997.02	-6661.42	-5388.31
0.196623	320051.1	86686.83	-6432.12	-1649.36	-6480.85	-4992
0.194545	320888.7	85896.74	-6336.11	-1546.28	-6426.4	-4873.29
0.189347	322985.1	83920.24	-6096.03	-1290.03	-6289.2	-4575.78
0.18931	323000	83906.23	-6094.33	-1288.23	-6288.22	-4573.67
0.178571	327332	79825.99	-5599.06	-766.459	-6000.5	-3956.96
0.171623	330136	77187.84	-5279.03	-434.096	-5811.23	-3556.3
0.169546	330974.5	76399.41	-5183.41	-335.507	-5754.16	-3436.26
0.164347	333073.1	74427.11	-4944.25	-90.3424	-5610.4	-3135.33
0.16431	333087.9	74413.13	-4942.55	-88.6121	-5609.37	-3133.2
0.153571	337424.4	70341.91	-4448.93	411.0298	-5307.93	-2509.05
0.146623	340231.5	67709.84	-4129.74	729.6481	-5109.64	-2103.28
0.144546	341071	66923.28	-4034.33	824.2181	-5049.85	-1981.66
0.139347	343171.9	64955.73	-3795.62	1059.515	-4899.21	-1676.7
0.13931	343186.8	64941.79	-3793.93	1061.177	-4898.14	-1674.53
0.128571	347528.4	60880.83	-3300.79	1541.325	-4582.2	-1041.54
0.121623	350339	58255.75	-2981.57	1848.002	-4374.26	-629.664
0.119546	351179.5	57471.34	-2886.1	1939.11	-4311.55	-506.156
0.114347	353283.2	55509.3	-2647.07	2165.97	-4153.48	-196.317
0.11431	353298.1	55495.4	-2645.38	2167.573	-4152.35	-194.117
0.103571	357645.7	51446.47	-2150.93	2631.381	-3820.53	449.6403
0.096623	360460.5	48829.71	-1830.31	2928.326	-3601.87	869.0405
0.094545	361302.2	48047.87	-1734.32	3016.662	-3535.87	994.8947
0.089347	363409.2	46092.49	-1493.8	3236.882	-3369.4	1310.811
0.08931	363424.2	46078.63	-1492.09	3238.439	-3368.21	1313.056
0.078571	367779.2	42044.47	-993.481	3689.99	-3018.11	1970.441
0.071623	370599.2	39438.14	-669.257	3980.176	-2786.83	2399.557
0.069545	371442.6	38659.57	-572.028	4066.691	-2716.91	2528.474
0.064347	373553.8	36712.71	-328.046	4282.795	-2540.31	2852.412
0.06431	373568.8	36698.92	-326.313	4284.326	-2539.05	2854.716
0.053571	377933.6	32684.27	181.3886	4729.66	-2166.23	3530.581
0.046623	380760.7	30092.23	513.2232	5017.794	-1918.63	3973.358
0.044545	381606.4	29318.25	613.0512	5104.056	-1843.52	4106.68
0.039347	383723.8	27383.64	864.3096	5320.369	-1653.21	4442.401
0.03931	383738.8	27369.94	866.0989	5321.905	-1651.84	4444.792
0.028571	388118.5	23385.01	1393.343	5772.498	-1246.34	5149.461
0.021623	390957.5	20816.79	1742.471	6068.904	-973.057	5615.488
0.019545	391807.2	20050.94	1848.484	6158.687	-889.275	5756.769
0.014347	393936.2	18139.5	2118.068	6386.722	-674.438	6115.244
0.01431	393951.3	18125.98	2120.005	6388.36	-672.884	6117.814
0.003571	398367.4	14213.87	2710.157	6888.513	-191.829	6894.479
2.50E-04	399746.4	13030.08	2918.055	7067.46	-16.6013	7160.844

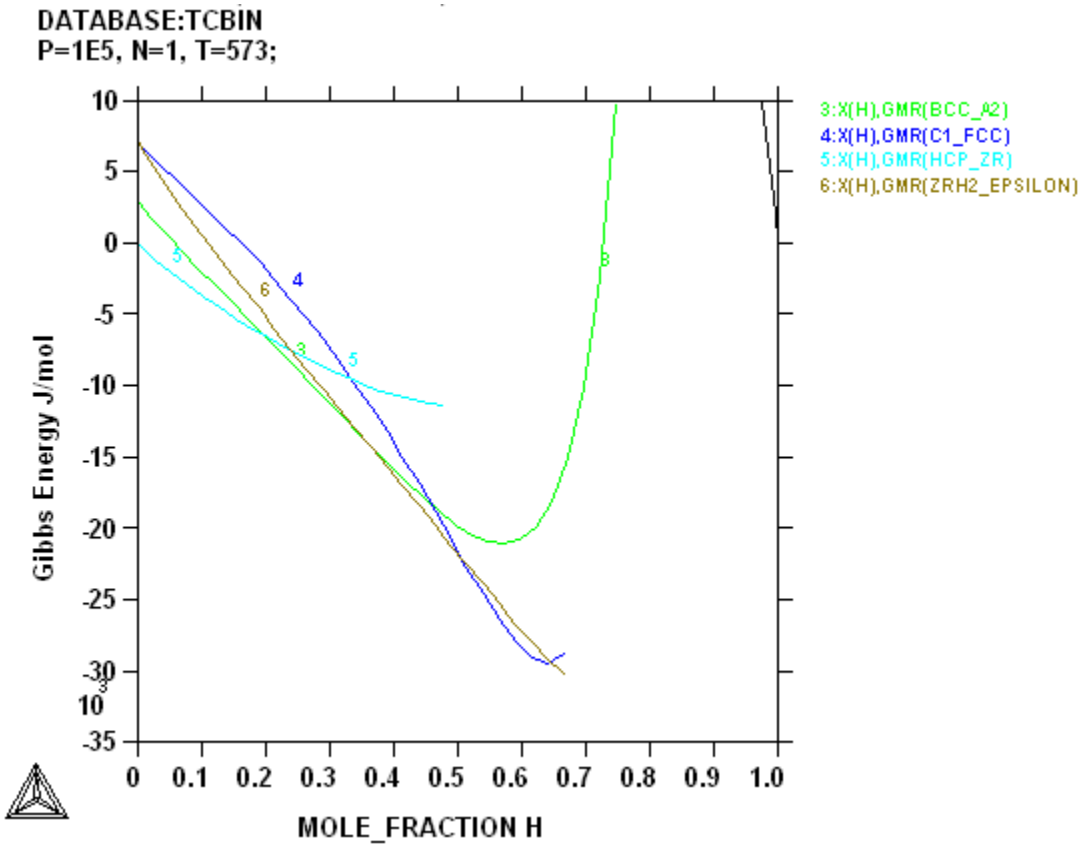

Figure A1 Thermodynamic properties of different phases at T=300°C

Table A2 Gibbs thermodynamic potentials of different phases in the Zr-H system at 350°C (in J/mole)

X(H)	GMR(GAS)	GMR(IONIC_LIQ)	GMR(BCC_A2)	GMR(C1_FCC)	GMR(HCP_ZR)	GMR(ZRH2_EPS)
0.99975	92.86265	399891.1	11864.89	-26248	-10024.1	-27958.6
0.994546	2069.708	397710.9	11864.89	-26248	-10024.1	-27958.6
0.969546	11692.54	387492.4	11864.89	-26248	-10024.1	-27958.6
0.944545	21378.83	377400.9	11864.89	-26248	-10024.1	-27958.6
0.919546	31097.11	367373.3	11864.89	-26248	-10024.1	-27958.6
0.894545	40837.6	357390.2	11864.89	-26248	-10024.1	-27958.6
0.869546	50595.4	347441.7	11864.89	-26248	-10024.1	-27958.6
0.844546	60367.55	337521.8	11864.89	-26248	-10024.1	-27958.6
0.819545	70152.08	327626.8	11864.89	-26248	-10024.1	-27958.6
0.794546	79947.58	317753.6	11864.89	-26248	-10024.1	-27958.6
0.769545	89753.02	307900.4	11864.89	-26248	-10024.1	-27958.6
0.746623	98751.7	298882	9749.115	-26248	-10024.1	-27958.6
0.744546	99567.59	298065.4	8553.437	-26248	-10024.1	-27958.6
0.721623	108574.1	289062.7	-1832.52	-26248	-10024.1	-27958.6
0.719546	109390.7	288247.5	-2575.93	-26248	-10024.1	-27958.6
0.696623	118404.6	279259.5	-9195.7	-26248	-10024.1	-27958.6
0.694545	119221.8	278445.6	-9673.32	-26248	-10024.1	-27958.6
0.671623	128242.7	269471.7	-13910.9	-26248	-10024.1	-27958.6
0.669546	129060.6	268659	-14214	-26248	-10024.1	-27958.6
0.664347	131107.4	266625.8	-14922.3	-26471.6	-10024.1	-27968.5
0.66431	131121.9	266611.4	-14927.1	-26474.5	-10024.1	-27968.1
0.646623	138088.2	259698.5	-16861.4	-27208	-10024.1	-27421.3
0.644545	138906.7	258887	-17046.2	-27239.3	-10024.1	-27337.7
0.639347	140955	256856.9	-17474.3	-27281.1	-10024.1	-27120.2
0.63931	140969.5	256842.5	-17477.1	-27281.2	-10024.1	-27118.7
0.621623	147940.8	249939.5	-18605.3	-27104.7	-10024.1	-26322
0.619546	148759.8	249129.2	-18708.4	-27057.3	-10024.1	-26224.7
0.614347	150809.6	247101.9	-18942.3	-26918.2	-10024.1	-25978.7
0.61431	150824.1	247087.6	-18943.8	-26917.2	-10024.1	-25976.9
0.596623	157800.3	240194.3	-19509.8	-26257.9	-10024.1	-25121.6
0.596623	157800.3	240194.3	-19509.8	-26257.9	-10024.1	-25121.6
0.594546	158619.9	239385.2	-19555.6	-26164.6	-10024.1	-25019.8
0.589347	160671	237360.7	-19653.2	-25918.8	-10024.1	-24764.1
0.58931	160685.5	237346.3	-19653.9	-25917	-10024.1	-24762.3
0.571623	167666.5	230462.6	-19823.2	-24968.6	-10024.1	-23885.1
0.569545	168486.6	229654.5	-19828.5	-24847.7	-10024.1	-23781.6
0.564347	170539.1	227632.8	-19829.4	-24537.9	-10024.1	-23522
0.56431	170553.7	227618.5	-19829.4	-24535.6	-10024.1	-23520.2
0.546623	177539.3	220744.1	-19716.7	-23416.2	-10024.1	-22634.1
0.544546	178360	219937.1	-19693	-23279.3	-10024.1	-22529.8
0.539347	180413.8	217918.1	-19625.1	-22932.6	-10024.1	-22268.7
0.53931	180428.4	217903.8	-19624.5	-22930.2	-10024.1	-22266.8
0.521623	187418.6	211038.6	-19310.4	-21716	-10024.1	-21376.9
0.519545	188239.8	210232.7	-19266	-21570.7	-10024.1	-21272.3
0.514347	190295.1	208216.4	-19148.7	-21205.1	-10024.1	-21010.4
0.51431	190309.7	208202.1	-19147.8	-21202.5	-10024.1	-21008.5
0.496623	197304.4	201346.2	-18689.5	-19944.3	-10142	-20116.7
0.494546	198126.2	200541.3	-18630.3	-19795.6	-10187.4	-20011.9
0.494546	198126.2	200541.3	-18630.3	-19795.6	-10187.4	-20011.9
0.489347	200182.8	198527.7	-18477.8	-19423	-10269.2	-19749.6
0.48931	200197.4	198513.5	-18476.7	-19420.3	-10269.6	-19747.7
0.478571	204446.6	194355.7	-18143.2	-18649.8	-10361.8	-19205.5
0.471623	207196.7	191666.7	-17915.5	-18151.6	-10388.7	-18854.4
0.469546	208019.1	190862.9	-17845.8	-18002.8	-10393.1	-18749.4
0.464347	210077	188852	-17668.2	-17631.1	-10397.8	-18486.6
0.46431	210091.6	188837.7	-17667	-17628.5	-10397.8	-18484.8
0.453571	214343.6	184685.6	-17287	-16863.7	-10383.4	-17941.6
0.446623	217095.5	182000.1	-17032.8	-16371.7	-10359.8	-17589.8
0.444545	217918.4	181197.5	-16955.7	-16225.1	-10350.8	-17484.6
0.439347	219977.7	179189.3	-16760.4	-15859.4	-10324.9	-17221.2
0.43931	219992.3	179175	-16759	-15856.8	-10324.7	-17219.4
0.428571	224247.1	175028.5	-16346.5	-15107.2	-10256.6	-16674.9
0.421623	227000.9	172346.7	-16073.8	-14626.6	-10203.2	-16322.2
0.419545	227824.3	171545.2	-15991.5	-14483.6	-10186	-16216.7
0.414347	229885	169539.7	-15783.9	-14127.4	-10140.4	-15952.6
0.41431	229899.6	169525.5	-15782.5	-14124.9	-10140.1	-15950.7
0.403571	234157.3	165384.7	-15347.5	-13396.4	-10035.3	-15404.5
0.396623	236912.9	162706.6	-15062.2	-12930.5	-9960.57	-15050.6
0.394546	237736.9	161906.1	-14976.3	-12792	-9937.23	-14944.7
0.389347	239798.9	159903.5	-14760.5	-12447.4	-9876.91	-14679.6
0.38931	239813.6	159889.3	-14758.9	-12444.9	-9876.47	-14677.7
0.378571	244074.2	155754.3	-14308.9	-11741.2	-9743.51	-14129.3
0.371623	246831.7	153080	-14015.2	-11291.9	-9651.84	-13773.9
0.369546	247656.2	152280.7	-13927	-11158.5	-9623.62	-13667.5

0.364347	249719.7	150280.9	-13705.8	-10826.6	-9551.39	-13401.2
0.36431	249734.3	150266.7	-13704.2	-10824.3	-9550.87	-13399.3
0.353571	253997.9	146137.7	-13244.5	-10147.3	-9394.66	-12848.2
0.346623	256757.4	143467.3	-12945.5	-9715.59	-9288.79	-12490.9
0.344546	257582.5	142669.1	-12855.9	-9587.48	-9256.43	-12384
0.339347	259647.5	140672.3	-12631.4	-9268.85	-9174.07	-12116.2
0.33931	259662.1	140658.1	-12629.8	-9266.6	-9173.48	-12114.3
0.328571	263928.8	136535.2	-12164.3	-8617.25	-8997.22	-11560
0.328571	263928.8	136535.2	-12164.3	-8617.25	-8997.22	-11560
0.321623	266690.2	133868.9	-11862.3	-8203.41	-8878.93	-11200.5
0.319545	267516	133071.9	-11771.9	-8080.65	-8842.94	-11092.9
0.314347	269582.5	131078.1	-11545.5	-7775.39	-8751.63	-10823.3
0.31431	269597.1	131064	-11543.9	-7773.24	-8750.98	-10821.4
0.303571	273866.9	126947.5	-11075.4	-7151.43	-8556.83	-10263.3
0.296623	276630.5	124285.3	-10771.9	-6755.31	-8427.36	-9901.28
0.294545	277456.9	123489.6	-10681.1	-6637.82	-8388.07	-9792.89
0.289347	279525	121499	-10453.9	-6345.72	-8288.63	-9521.33
0.28931	279539.6	121484.9	-10452.3	-6343.66	-8287.92	-9519.41
0.278571	283812.8	117375	-9982.68	-5748.76	-8077.37	-8956.99
0.271623	286578.6	114717.3	-9678.75	-5369.83	-7937.54	-8591.99
0.269546	287405.6	113922.9	-9587.88	-5257.45	-7895.2	-8482.69
0.264347	289475.3	111935.6	-9360.51	-4978.04	-7788.16	-8208.84
0.26431	289490	111921.6	-9358.9	-4976.07	-7787.4	-8206.89
0.253571	293766.7	107818.7	-8889.32	-4407	-7561.45	-7639.52
0.246623	296534.8	105165.6	-8585.59	-4044.49	-7411.83	-7271.16
0.244546	297362.6	104372.7	-8494.81	-3936.96	-7366.58	-7160.84
0.239347	299434.1	102389	-8267.68	-3669.6	-7252.31	-6884.36
0.23931	299448.8	102374.9	-8266.07	-3667.72	-7251.49	-6882.4
0.228571	303729.2	98279.54	-7797.15	-3123.06	-7010.76	-6309.38
0.221623	306499.8	95631.41	-7493.91	-2775.98	-6851.66	-5937.2
0.219546	307328.2	94839.96	-7403.28	-2673.01	-6803.59	-5825.71
0.214347	309401.7	92860.06	-7176.54	-2416.93	-6682.28	-5546.25
0.21431	309416.4	92846.03	-7174.94	-2415.12	-6681.42	-5544.27
0.203571	313700.9	88758.75	-6706.81	-1893.19	-6426.19	-4964.82
0.196623	316474.2	86116	-6404.06	-1560.39	-6257.73	-4588.29
0.194545	317303.4	85326.19	-6313.57	-1461.62	-6206.86	-4475.46
0.189347	319378.9	83350.43	-6087.15	-1215.92	-6078.54	-4192.6
0.18931	319393.7	83336.43	-6085.55	-1214.18	-6077.63	-4190.59
0.178571	323682.6	79257.97	-5617.94	-713.029	-5807.87	-3603.79
0.171623	326458.8	76621.13	-5315.4	-393.182	-5629.95	-3222.26
0.169546	327289	75833.12	-5224.94	-298.21	-5576.24	-3107.9
0.164347	329366.8	73861.95	-4998.56	-61.8437	-5440.78	-2821.11
0.16431	329381.5	73847.97	-4996.96	-60.1744	-5439.81	-2819.07
0.153571	333675.3	69779.32	-4529.14	422.4332	-5155.14	-2223.78
0.146623	336454.8	67149.1	-4226.22	730.8433	-4967.41	-1836.44
0.144546	337286.1	66363.12	-4135.61	822.4854	-4910.74	-1720.29
0.139347	339366.4	64397.11	-3908.76	1050.706	-4767.81	-1428.92
0.13931	339381.2	64383.17	-3907.15	1052.318	-4766.79	-1426.85
0.128571	343680.5	60325.67	-3437.9	1518.985	-4466.35	-821.573
0.121623	346463.9	57703.06	-3133.66	1817.754	-4268.14	-427.349
0.119546	347296.2	56919.41	-3042.6	1906.622	-4208.29	-309.073
0.114347	349379.6	54959.39	-2814.46	2128.129	-4057.28	-12.2381
0.11431	349394.4	54945.5	-2812.84	2129.695	-4056.2	-10.1292
0.103571	353700.3	50901.08	-2340.2	2583.598	-3738.49	607.1974
0.096623	356488.2	48287.51	-2033.19	2874.966	-3528.62	1009.819
0.094545	357322	47506.67	-1941.19	2961.763	-3465.19	1130.708
0.089347	359408.9	45553.87	-1710.49	3178.392	-3305.05	1434.309
0.08931	359423.8	45540.04	-1708.85	3179.925	-3303.91	1436.467
0.078571	363737.7	41511.68	-1229.76	3625.259	-2966.33	2068.927
0.071623	366531.2	38909.43	-917.604	3912.302	-2742.74	2482.311
0.069545	367366.8	38132.15	-823.891	3998.015	-2675.05	2606.589
0.064347	369458.4	36188.63	-588.516	4212.394	-2503.89	2919.056
0.06431	369473.2	36174.86	-586.843	4213.914	-2502.66	2921.279
0.053571	373797.8	32167.71	-96.0059	4657.013	-2140.38	3574.123
0.046623	376599.1	29581.02	225.6262	4944.7	-1899.04	4002.544
0.044545	377437.1	28808.72	322.5214	5030.988	-1825.72	4131.664
0.039347	379535.4	26878.52	566.6954	5247.709	-1639.65	4457.076
0.03931	379550.3	26864.85	568.4358	5249.25	-1638.31	4459.396
0.028571	383891	22890.01	1082.337	5702.366	-1240.5	5143.825
0.021623	386705.2	20329.21	1423.934	6001.778	-971.238	5597.693
0.019545	387547.7	19565.76	1527.901	6092.704	-888.479	5735.518
0.014347	389658.6	17660.74	1792.86	6324.181	-675.745	6085.792
0.01431	389673.6	17647.27	1794.767	6325.846	-674.204	6088.308
0.003571	394053.9	13751.6	2378.827	6836.931	-194.244	6851.265
2.50E-04	395422.9	12575.19	2587.204	7021.72	-17.0472	7115.692

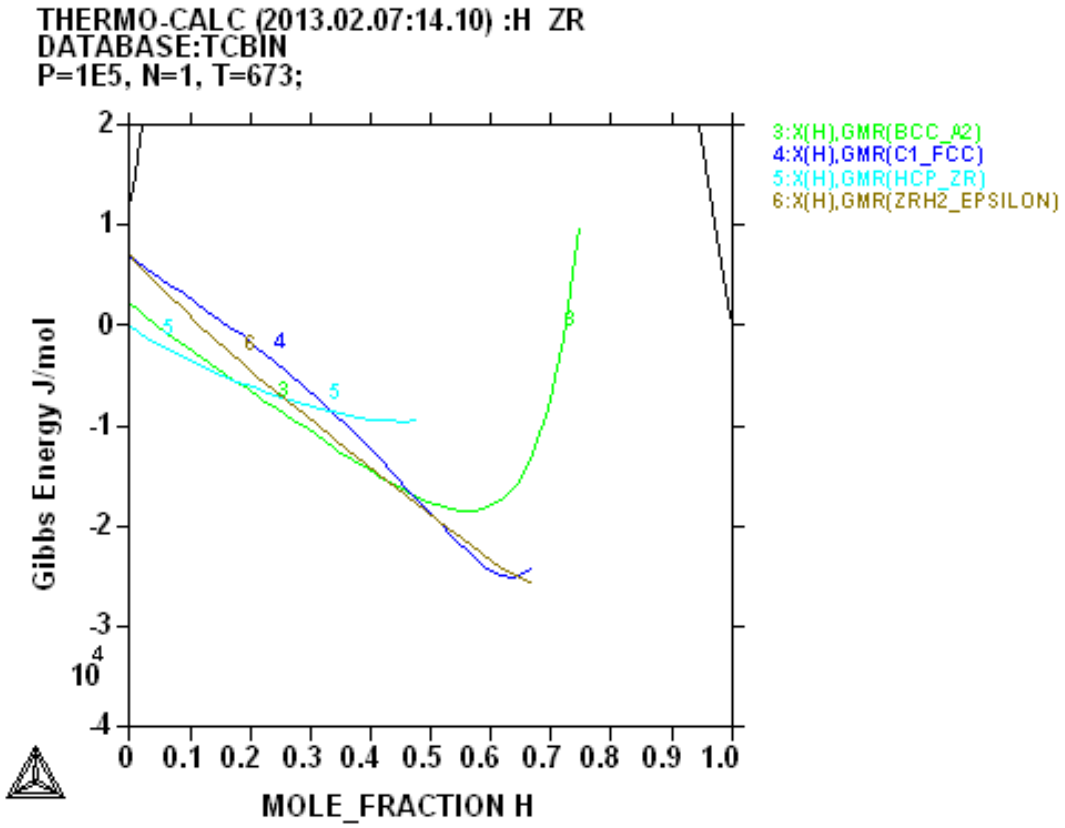

Figure A2 Thermodynamic properties of different phases at T=350°C

Table A3 Gibbs thermodynamic potentials of different phases in the Zr-H system at 400°C (in J/mole)

X(H)	GMR(GAS)	GMR(IONIC_LIQ)	GMR(BCC_A2)	GMR(C1_FCC)	GMR(HCP_ZR)	GMR(ZRH2_EPS)
0.99975	91.30695	399890	11785.57	-23957.6	-8984.1	-25635.4
0.99975	91.30695	399890	11785.57	-23957.6	-8984.1	-25635.4
0.994546	2039.309	397694.3	11785.57	-23957.6	-8984.1	-25635.4
0.979762	7641.181	391594.6	11785.57	-23957.6	-8984.1	-25635.4
0.969546	11533.82	387421.9	11785.57	-23957.6	-8984.1	-25635.4
0.954762	17183.74	381418.3	11785.57	-23957.6	-8984.1	-25635.4
0.944545	21096.89	377286.7	11785.57	-23957.6	-8984.1	-25635.4
0.929762	26769.05	371327.4	11785.57	-23957.6	-8984.1	-25635.4
0.919546	30694.51	367220.4	11785.57	-23957.6	-8984.1	-25635.4
0.904762	36381.69	361291.3	11785.57	-23957.6	-8984.1	-25635.4
0.894545	40316.14	357202.2	11785.57	-23957.6	-8984.1	-25635.4
0.879762	46014.84	351296.1	11785.57	-23957.6	-8984.1	-25635.4
0.869546	49956.46	347221.4	11785.57	-23957.6	-8984.1	-25635.4
0.854762	55664.64	341334.3	11785.57	-23957.6	-8984.1	-25635.4
0.844546	59612.29	337271.7	11785.57	-23957.6	-8984.1	-25635.4
0.829762	65328.58	331400.7	11785.57	-23957.6	-8984.1	-25635.4
0.819545	69281.48	327348.6	11785.57	-23957.6	-8984.1	-25635.4
0.804762	75004.94	321492	11785.57	-23957.6	-8984.1	-25635.4
0.794546	78962.52	317449.2	11785.57	-23957.6	-8984.1	-25635.4
0.779762	84692.45	311605.5	11785.57	-23957.6	-8984.1	-25635.4
0.769545	88654.31	307571.3	11785.57	-23957.6	-8984.1	-25635.4
0.754762	94390.16	301739.5	11785.57	-23957.6	-8984.1	-25635.4
0.746623	97549.43	298531.7	9762.562	-23957.6	-8984.1	-25635.4
0.744546	98355.97	297713.2	8624.618	-23957.6	-8984.1	-25635.4
0.729762	104097.3	291892.4	1796.645	-23957.6	-8984.1	-25635.4
0.721623	107259.5	288690.4	-1233.94	-23957.6	-8984.1	-25635.4
0.719546	108066.8	287873.4	-1939.52	-23957.6	-8984.1	-25635.4
0.704762	113813.4	282063	-6280.14	-23957.6	-8984.1	-25635.4
0.696623	116978.4	278866.7	-8231.13	-23957.6	-8984.1	-25635.4
0.694545	117786.4	278051.1	-8686.04	-23957.6	-8984.1	-25635.4
0.679762	123537.9	272250.5	-11482.5	-23957.6	-8984.1	-25635.4
0.671623	126705.5	269059.4	-12733.5	-23957.6	-8984.1	-25635.4
0.669546	127514.2	268245.2	-13024.1	-23957.6	-8984.1	-25635.4
0.664347	129538	266208.2	-13704	-24191.8	-8984.1	-25669.6
0.66431	129552.3	266193.7	-13708.6	-24194.8	-8984.1	-25669.6
0.654762	133270.3	262454	-14795.2	-24740.2	-8984.1	-25500.4
0.646623	136440.5	259268.1	-15574.3	-24981.9	-8984.1	-25254.8
0.644545	137249.9	258455.1	-15753.5	-25020.2	-8984.1	-25184.7
0.639347	139275.3	256421.3	-16169.6	-25081	-8984.1	-25000.2
0.63931	139289.6	256406.9	-16172.4	-25081.2	-8984.1	-24998.9
0.629762	143010.6	252673.1	-16824.6	-25079	-8984.1	-24634.7
0.621623	146183.3	249492	-17278.5	-24980.6	-8984.1	-24306.4
0.619546	146993.2	248680.3	-17380.6	-24943.2	-8984.1	-24220.7
0.614347	149020.2	246649.6	-17613.6	-24830.1	-8984.1	-24003.3
0.61431	149034.5	246635.2	-17615.2	-24829.2	-8984.1	-24001.8
0.604762	152758.3	242907.1	-17964.7	-24556	-8984.1	-23593.9
0.596623	155933.4	239730.8	-18190.8	-24266.1	-8984.1	-23239.5
0.596623	155933.4	239730.8	-18190.8	-24266.1	-8984.1	-23239.5
0.594546	156744	238920.4	-18238.8	-24184.7	-8984.1	-23148.3
0.589347	158772.4	236892.7	-18343	-23969.4	-8984.1	-22918.8
0.58931	158786.8	236878.4	-18343.7	-23967.8	-8984.1	-22917.2
0.579762	162513.4	233155.8	-18479.4	-23532.7	-8984.1	-22491.8
0.571623	165690.8	229984.2	-18544.1	-23127.4	-8984.1	-22126.1
0.569545	166502	229175	-18553.7	-23019.6	-8984.1	-22032.4
0.564347	168532	227150.3	-18566.4	-22742.6	-8984.1	-21797.3
0.56431	168546.3	227135.9	-18566.4	-22740.6	-8984.1	-21795.7
0.554762	172275.7	223418.8	-18549.9	-22208.4	-8984.1	-21361.9
0.546623	175455.4	220251.9	-18499.2	-21734.7	-8984.1	-20990.6
0.544546	176267.1	219443.8	-18481.3	-21611.2	-8984.1	-20895.6
0.539347	178298.6	217422.1	-18428.4	-21298.3	-8984.1	-20657.6
0.53931	178313	217407.7	-18428	-21296	-8984.1	-20655.9
0.529762	182045	213696	-18302.2	-20708.3	-8984.1	-20217.6
0.521623	185227	210533.7	-18168.8	-20196.6	-8984.1	-19843
0.519545	186039.3	209726.7	-18131.1	-20064.7	-8984.1	-19747.3
0.514347	188072.2	207707.9	-18031.1	-19732.6	-8984.1	-19507.5
0.51431	188086.7	207693.6	-18030.3	-19730.2	-8984.1	-19505.8
0.504762	191821.3	203987.2	-17826	-19114.3	-8984.1	-19064.5
0.504762	191821.3	203987.2	-17826	-19114.3	-8984.1	-19064.5
0.496623	195005.7	200829.5	-17632.9	-18584.7	-9123.9	-18687.6
0.494546	195818.5	200023.7	-17581.1	-18449.1	-9180.63	-18591.3
0.494546	195818.5	200023.7	-17581.1	-18449.1	-9180.63	-18591.3
0.489347	197852.9	198007.8	-17447.1	-18109.1	-9288.11	-18350.2
0.48931	197867.3	197993.5	-17446.1	-18106.7	-9288.75	-18348.5
0.479762	201604.7	194292.5	-17185.2	-17480.7	-9416.26	-17904.8
0.478571	202070.8	193831.2	-17151.5	-17402.6	-9427.97	-17849.5
0.471623	204791.3	191139.3	-16949.3	-16946.8	-9482.63	-17526
0.469546	205604.8	190334.7	-16887.2	-16810.6	-9495.02	-17429.2
0.464347	207640.6	188321.7	-16728.9	-16470.1	-9519.26	-17186.9
0.46431	207655	188307.4	-16727.7	-16467.7	-9519.4	-17185.1

0.454762	211395.1	184611.7	-16426.3	-15843.9	-9542.32	-16739.3
0.453571	211861.4	184151.1	-16387.8	-15766.3	-9543.48	-16683.6
0.446623	214583.9	181463.1	-16159.6	-15314.5	-9543.6	-16358.6
0.444545	215398	180659.7	-16090.3	-15179.8	-9541.59	-16261.3
0.439347	217435.3	178649.6	-15914.5	-14843.7	-9532.75	-16017.6
0.43931	217449.7	178635.4	-15913.3	-14841.3	-9532.67	-16015.9
0.429762	221192.5	174945.1	-15582.9	-14227.6	-9503.46	-15567.7
0.428571	221659.2	174485.1	-15541.1	-14151.5	-9498.74	-15511.8
0.421623	224383.7	171801.1	-15294.5	-13708.7	-9466.76	-15184.9
0.419545	225198.3	170998.8	-15219.9	-13576.9	-9455.79	-15087.1
0.414347	227237.1	168991.8	-15031.9	-13248.4	-9425.69	-14842.1
0.41431	227251.5	168977.5	-15030.5	-13246.1	-9425.46	-14840.3
0.404762	230997	165292.8	-14679.8	-12647.6	-9360.79	-14389.5
0.403571	231464.1	164833.5	-14635.7	-12573.5	-9351.93	-14333.2
0.396623	234190.6	162153.4	-14376.1	-12142.8	-9296.83	-14004.3
0.394546	235005.8	161352.4	-14297.9	-12014.8	-9279.29	-13905.9
0.389347	237046.1	159348.3	-14101.3	-11695.8	-9233.29	-13659.3
0.38931	237060.6	159334.1	-14099.9	-11693.6	-9232.96	-13657.6
0.379762	240808.8	155654.9	-13735.1	-11113.5	-9141.04	-13203.8
0.378571	241276.3	155196.3	-13689.3	-11041.7	-9128.94	-13147.1
0.371623	244004.8	152520.4	-13420.8	-10625	-9055.55	-12816
0.369546	244820.7	151720.6	-13340.2	-10501.2	-9032.72	-12716.9
0.364347	246862.5	149719.6	-13137.7	-10193	-8973.88	-12468.5
0.36431	246877	149705.5	-13136.3	-10190.8	-8973.45	-12466.8
0.354762	250628.1	146031.9	-12761.9	-9630.84	-8859.12	-12009.6
0.353571	251095.9	145574.1	-12715	-9561.57	-8844.31	-11952.5
0.346623	253826.5	142902.3	-12440.6	-9159.76	-8755.58	-11618.9
0.344546	254643	142103.8	-12358.3	-9040.44	-8728.29	-11519
0.339347	256686.4	140106	-12151.9	-8743.54	-8658.5	-11268.7
0.33931	256700.9	140091.9	-12150.4	-8741.44	-8658	-11266.9
0.329762	260455	136424.2	-11769.8	-8202.31	-8524.35	-10806
0.328571	260923.1	135967.1	-11722.2	-8135.66	-8507.2	-10748.4
0.328571	260923.1	135967.1	-11722.2	-8135.66	-8507.2	-10748.4
0.321623	263655.9	133299.8	-11443.9	-7749.07	-8405.06	-10411.9
0.319545	264473.1	132502.5	-11360.5	-7634.32	-8373.84	-10311.1
0.314347	266518.2	130508	-11151.6	-7348.81	-8294.38	-10058.6
0.31431	266532.7	130493.9	-11150.2	-7346.79	-8293.81	-10056.8
0.304762	270289.8	126832.4	-10765.5	-6828.54	-8142.95	-9591.66
0.303571	270758.3	126376	-10717.5	-6764.48	-8123.7	-9533.55
0.296623	273493.4	123713.2	-10436.8	-6392.99	-8009.47	-9193.82
0.294545	274311.2	122917.3	-10352.8	-6282.72	-7974.69	-9092.06
0.289347	276358	120926.3	-10142.4	-6008.42	-7886.44	-8837.06
0.28931	276372.5	120912.1	-10140.9	-6006.48	-7885.81	-8835.25
0.279762	280132.9	117257.1	-9753.87	-5508.61	-7719.16	-8365.43
0.278571	280601.8	116801.5	-9705.57	-5447.07	-7697.98	-8306.72
0.271623	283339.2	114143.4	-9423.47	-5090.21	-7572.57	-7963.42
0.269546	284157.8	113349	-9339.07	-4984.29	-7534.49	-7860.58
0.264347	286206.4	111361.5	-9127.77	-4720.77	-7438.04	-7602.81
0.26431	286220.9	111347.5	-9126.28	-4718.9	-7437.35	-7600.98
0.254762	289984.6	107699.1	-8737.84	-4240.56	-7255.89	-7125.92
0.253571	290454	107244.4	-8689.38	-4181.42	-7232.88	-7066.54
0.246623	293193.9	104591.3	-8406.43	-3838.47	-7096.88	-6719.27
0.244546	294013.2	103798.4	-8321.8	-3736.65	-7055.67	-6615.22
0.239347	296063.8	101814.8	-8109.96	-3483.33	-6951.4	-6354.37
0.23931	296078.3	101800.7	-8108.46	-3481.54	-6950.66	-6352.52
0.229762	299845.6	98159.59	-7719.12	-3021.54	-6754.99	-5871.61
0.228571	300315.4	97705.81	-7670.55	-2964.66	-6730.22	-5811.48
0.221623	303058.1	95058.09	-7387	-2634.69	-6583.99	-5459.77
0.219546	303878.2	94266.8	-7302.2	-2536.7	-6539.72	-5354.36
0.214347	305930.8	92287.31	-7089.92	-2292.84	-6427.85	-5090.06
0.21431	305945.3	92273.28	-7088.41	-2291.11	-6427.05	-5088.19
0.204762	309716.5	88639.87	-6698.26	-1848.05	-6217.46	-4600.72
0.203571	310186.8	88187.07	-6649.59	-1793.24	-6190.96	-4539.75
0.196623	312932.3	85545.17	-6365.4	-1475.16	-6034.61	-4183.05
0.194545	313753.3	84755.64	-6280.39	-1380.66	-5987.32	-4076.12
0.189347	315808.1	82780.62	-6067.58	-1145.4	-5867.88	-3807.94
0.18931	315822.7	82766.62	-6066.07	-1143.74	-5867.03	-3806.03
0.179762	319598.1	79141.66	-5674.8	-715.951	-5643.49	-3311.16
0.178571	320069	78689.95	-5625.98	-662.995	-5615.24	-3249.24
0.171623	322817.7	76054.43	-5340.82	-355.532	-5448.68	-2886.88
0.169546	323639.7	75266.84	-5255.5	-264.137	-5398.32	-2778.22
0.164347	325697	73296.77	-5041.84	-36.471	-5271.16	-2505.61
0.16431	325711.6	73282.81	-5040.33	-34.8622	-5270.25	-2503.68
0.154762	329491.7	69667.25	-4647.26	379.5681	-5032.4	-2000.33
0.153571	329963.1	69216.73	-4598.19	430.9154	-5002.35	-1937.33
0.146623	332715.4	66588.36	-4311.44	729.2496	-4825.19	-1568.46
0.144546	333538.5	65802.97	-4225.6	818.0032	-4771.63	-1457.79
0.139347	335598.6	63838.48	-4010.55	1039.246	-4636.41	-1180.07
0.13931	335613.2	63824.55	-4009.02	1040.81	-4635.44	-1178.09
0.129762	339398.6	60219.66	-3612.98	1444.165	-4382.47	-664.886
0.128571	339870.7	59770.52	-3563.49	1494.2	-4350.51	-600.608
0.121623	342627.1	57150.36	-3274.16	1785.192	-4162.02	-224.089

0.119546	343451.5	56367.49	-3187.47	1871.86	-4105.03	-111.062
0.114347	345514.8	54409.48	-2970.15	2088.113	-3961.07	172.7289
0.11431	345529.4	54395.6	-2968.61	2089.643	-3960.05	174.7458
0.104762	349321.1	50803.22	-2567.77	2484.752	-3690.53	699.7462
0.103571	349794.1	50355.69	-2517.63	2533.846	-3656.46	765.5587
0.096623	352555.4	47745.31	-2224.14	2819.769	-3455.38	1151.348
0.094545	353381.2	46965.46	-2136.1	2905.065	-3394.52	1267.256
0.089347	355448.4	45015.26	-1915.15	3118.202	-3240.7	1558.501
0.08931	355463.1	45001.44	-1913.58	3119.711	-3239.61	1560.572
0.079762	359262.4	41424.39	-1505.08	3510.368	-2951.09	2100.276
0.078571	359736.4	40978.88	-1453.88	3559.034	-2914.55	2168.023
0.071623	362503.8	38380.74	-1153.7	3843.066	-2698.64	2565.621
0.069545	363331.6	37604.73	-1063.47	3928.016	-2633.18	2685.244
0.064347	365403.8	35664.55	-836.635	4140.769	-2467.46	2986.2
0.06431	365418.5	35650.8	-835.021	4142.278	-2466.28	2988.342
0.054762	369228	32093.96	-413.876	4534.298	-2154.2	3547.694
0.053571	369703.3	31651.15	-360.907	4583.346	-2114.54	3618.081
0.046623	372479.1	29069.8	-49.3855	4870.718	-1879.46	4032.091
0.044545	373309.6	28299.19	44.6044	4957.073	-1807.92	4156.995
0.039347	375389	26373.39	281.7625	5174.302	-1626.09	4472.057
0.03931	375403.7	26359.75	283.4545	5175.849	-1624.78	4474.304
0.029762	379228.5	22833.52	727.8063	5580.555	-1278.99	5063.785
0.028571	379705.9	22395.01	784.1545	5631.69	-1234.66	5138.411
0.021623	382495.8	19841.64	1118.313	5934.24	-969.42	5580.066
0.019545	383331	19080.57	1220.26	6026.35	-887.682	5714.419
0.014347	385424	17181.98	1480.664	6261.367	-677.052	6056.453
0.01431	385438.9	17168.56	1482.542	6263.061	-675.523	6058.912
0.004762	389299.9	13714.7	1992.044	6723.095	-254.497	6720.349
0.003571	389783.9	13289.34	2060.651	6785.281	-196.658	6808.079
2.50E-04	391143.2	12120.3	2269.551	6975.975	-17.4931	7070.542

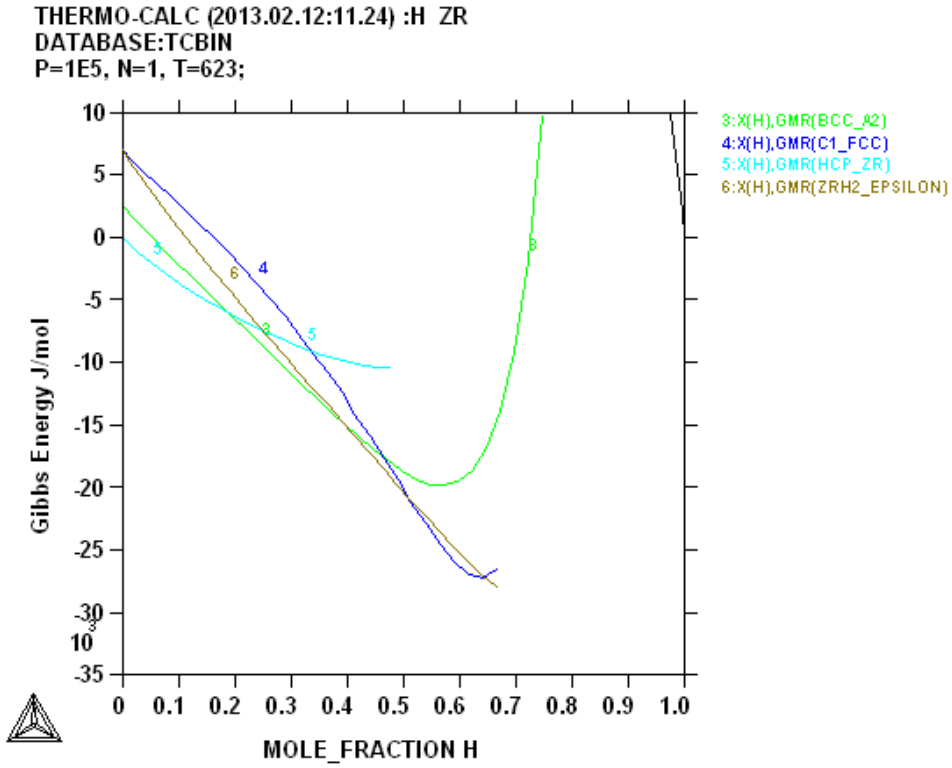

Figure A3 Thermodynamic properties of different phases at T=400°C